Effect of Microstructure on the Static and Dynamic Behavior of Recycled Asphalt Material

Martin H. Sadd, Professor
Qingli Dai, Research Assistant

May 2001

URI-TC Project No. 536108

Prepared For

University of Rhode Island
Transportation Center

DISCLAIMER

1. Report No	2. Government Accession No.	3. Recipient's Catalog No.
URITC 99-8	IN/A	N/A

4. Title and Subtitle	5. Report Date
Effect of Microstructure on the Static and Dynamic Behavior of Recycled Asphalt Materials	May 2001
	6. Performing Organization Code: N/A

7. Authors(s)	8. Performing Organization Report No.
Martin H. Sadd and Qingli Dai	

9. Performing Organization Name and Address	10. Work Unit No. (TRAIS)
University of Rhode Island Mechanical Engineering & Applied Mechanics Department 92 Upper College Road Kingston, RI 02881	N/A
	11. Contract or Grant No.: 536108
	13. Type of Report and Period Covered: Final

12. Sponsoring Agency Name and Address	14. Sponsoring Agency Code
University of Rhode Island Transportation Center Kingston, RI 02881	URITC 99-8 A Study Conducted in Cooperation With the U.S. DOT

15. Supplementary Notes
N/A

16. Abstract
This report describes the first year's research activities of a project dealing with the behavior of recycled asphalt pavement (RAP). The project's primary interest is to relate particular microstructural and recycling parameters to the material's mechanical response. The first year was devoted to the development of a theoretical/numerical modeling scheme. Future work will involve both theoretical/numerical and experimental studies. The numerical model was developed using the finite element method, whereby the microstructural asphalt/binder system was replaced by an equivalent finite element network. Special elements in the network are developed and these represent the load carrying behavior between neighboring aggregate pairs. Based on this modeling work, a computer simulation code (FEAMS) was created. Also developed was a material generating code (AMGEN), which can create an aggregate-binder model system with varying degrees of microstructure. Development of the finite element model and the material generating procedure are discussed in detail. Comparative verification computer runs on single element and 4-cell aggregate structures are presented. Finally, model simulations of standard laboratory experiments including compression and indirect tension tests are given. Although the results are preliminary, they do indicate that the modeling scheme provides useful comparisons and information that can be applied to RAP materials.

17. Key Words	18. Distribution Statement
Recycled Asphalt, Finite Element Modeling, Asphalt Microstructure, Numerical Simulation	No restrictions. This document is available to the public through the University of Rhode Island Transportation Center, 85 Briar Lane, Kingston, RI 02881

19. Security Classif. (of this report)	20. Security Classif. (of this page)	21. No. of Pages	22. Price
Unclassified	Unclassified	45	N/A

Form DOT F 1700.7 (8-72) Reproduction of completed page authorized (art. 5/94)

TABLE OF CONTENTS

ABSTRACT

This report describes the first year's research activities of a project dealing with the behavior of recycled asphalt materials (RAP). The project's primary interest is to relate particular microstructural and recycling parameters to the material's mechanical response. The first year was devoted to the development of a theoretical/numerical modeling scheme. Future work will involve both theoretical/numerical and experimental studies. The numerical model was developed using the finite element method, whereby the microstructural asphalt/binder system was replaced by an equivalent finite element network. Special elements in the network are developed and these represent the load carrying behavior between neighboring aggregate pairs. Based on this modeling work, a computer simulation code (FEAMS) was created. Our modeling has also developed a material generating code (AMGEN), which can create an aggregate-binder system with varying degrees of microstructure. Development of the finite element model and the material generating procedure are discussed in detail. Comparative verification computer runs on single element and 4-cell aggregate structures are presented. Finally, model simulations of standard laboratory experiments including compression and indirect tension tests are given. Although the results are preliminary, they do indicate that the modeling scheme provides useful comparisons and information that can be applied to recycled asphalt materials.

1. INTRODUCTION

Because of its environmentally friendly nature and promise for cost savings, there exists considerable state, national and international interest in the use of recycled asphalt pavement materials (RAP). Such use of recycled materials has been occurring with varying degrees of success in the United States for the past 20 years. In 1998 the U.S. Congress established the Recycled Materials Resource Center (RMRC) at the Universtiy of New Hampshire. The purpose of the Center was to use research and outreach to reduce barriers to recycling in road construction. Just recently the Federal Highway Administration completed a report by Schimmoller, et.al. (1) of a scanning tour of recycling activities in several European countries. This report was presented at the last Transportation Research Board meeting in January 2001. These activities clearly indicate the strong national interest in the appropriate use of recycled products for roadways.

Both hot and cold mix recycled materials exhibit different mechanical properties when compared with new pavement product. In some cases the performance of RAP materials has not been as good, while in other cases the recycled product had better structural performance, Kandhal, et.al. (2). For Cold In-Place Recycling (CIR), recent work by Brayton, et.al. (3) has investigated performanced-based mix-designs in an effort to provide information on the proper use of such materials. However, there still exists uncertainty on proper recycling processes and on the subsequent performance of the recycled product. Asphalt is a complex heterogeneous material composed of aggregate, binder/cement, additives and void space. Recycling processes further complicate the mechanical behavior by introducing additional variation of these constituents, and by adding several ageing/time-dependent effects such as hardening, chemical oxidation and binder microcracking. A fundamental understanding of the material behavior is

needed to help understand and explain recycling issues, and a micromechanical model would be best to establish such basic mechanisms.

During service, asphalt pavements must withstand a wide variety of loading and temperature conditions. For example, traffic loadings can vary from quasi-static to dynamic impact, and pavement breakdown commonly occurs as a result of strength (stress), fracture and/or fatigue failure, and time dependent deformation (creep-rutting). Early studies on the mechanical and fracture behaviors of asphalt and bituminous cements include the work of Salam and Monismith (4), Majidzaheh and Kauffmann (5), Majidzadeh et.al. (6), Karakouzian and Majidzadeh (7), and Sousa and Monismith (8). With regard to recycled materials, Sulaiman and Stock (9) have conducted fracture experiments on RAP materials with varying amounts of recycled constituent. Most recently Venkatram (10) conducted a series of fracture and dynamic impact experiments on RAP materials.

As mentioned, asphalt is a multiphase, heterogeneous material composed of aggregate particles, binder cementation and open void space. Previous studies focusing on the continuum response of asphalt materials cannot be used to describe the micromechanical behavior between aggregate and binder. Recently some studies have been investigating the micromechanical behaviors of particulate, porous and heterogeneous materials. For example, studies on cemented particulate materials by Dvorkin et.al. (11) and Zhu et.al. (12,13) provide information on the load transfer between particles which are cemented together. Such mechanics provide details on the normal and tangential interparticle load transfer, and would be fundamental in developing a micromechanical theory for load distribution and failure of such materials. Some contact-based analysis of asphalt performance has recently been reported by Zhu et.al. (14,15). Using mixture theory, Krishnan and Rao (16) presented a multi-phase approach to explain air void reduction in asphalt materials under load.

Recent numerical modeling of cemented particulate materials has generally used two particular simulation schemes. The first method uses *finite element* procedures to establish the load carrying behavior between the particles. A second general approach incorporates the *discrete element method*, which models the individual motion of each particle in model granular systems.

Discrete element modeling studies on cemented particulate materials include the work by Rothenburg, et.al. (17), Chang and Meegoda (18), Trent and Margolin (19), Buttlar and You (20) and Ullidtz (21). Sadd et.al. (22,23) have also used this scheme to numerically investigated the dynamic response of cemented and damaged granular materials.

In regard to finite element modeling (FEM), Stankowski (24) applied standard FEM techniques to cemented particulate composites, while Liao and Chang (25) established a FEM scheme for particulate materials with no cementation. A general finite element approach to simulate particulate material systems has used the idea of representing the interparticle behavior using an *equivalent lattice network system.* This type of microstructural modeling has been used previously; see for example Bazant, et.al. (26), Sadd et.al. (27) and Budhu, et.al. (28). Recently, Mustoe and Griffiths (29) developed a finite element model, which was equivalent to a particular discrete element approach. They pointed out that the FEM model has an advantage over the discrete element scheme for static problems.

Based on the review of past modeling work, the finite element scheme appeared to be most suited for developing an asphalt simulation model. Recycling will obviously affect the cemenatation/binder properties and the cohesion response between binder and aggregate, and these particular behaviors are of prime interest in the study. Using fundamental modeling at the micromechanical level, emphasis was placed on particular aggregate-binder behaviors which most directly affect the overall mechanical properties of the material and which are related to

recycling processes. Current research results for the first year include the development of two computer codes: one for generating model material systems and one for conducting mechanical asphalt simulation of the generated models. Results using each of these codes are presented.

2. ASPHALT MATERIAL MODELING

Bituminous asphalt can be described as a multi-phase material containing aggregate, binder cement (including mastic and fine particles) and air voids (see Figure 1). The load transfer between the aggregates plays a primary role in determining the load carrying capacity and failure of such complex materials. Our goal is to develop a numerical micromechanical

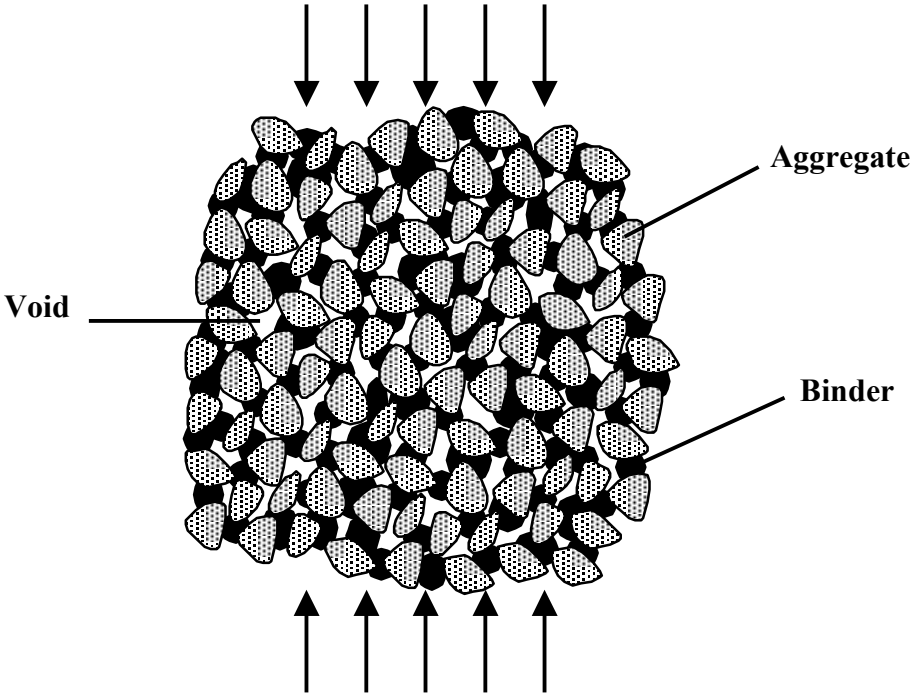

FIGURE 1 Schematic of multi-phase asphalt materials.

model of such materials by properly accounting for the load transfer between all aggregates in an idealized cemented particulate system. The aggregate material is normally much stiffer than the binder, and thus aggregates are to be modeled as rigid particles. On the other hand, the softer binder cement material usually gives a time-dependent viscoelastic response under loading. Additionally, binder behavior also can include hardening, debonding and microcracking, and

these lead to many complicated failure mechanisms. Therefore, asphalt materials provide great challenges to develop models that can adequately predict such failures.

In order to properly account for the load transfer between aggregates in an idealized system, we assume that there is an effective binder zone between neighboring particles. It is through this zone that the micro-mechanical load transfer occurs between each aggregate pair. This loading can be reduced to a resultant force and moment system as shown in Figure 2. The resultant force loading on a given aggregate can be reduced to normal and tangential components with respect to a coordinate system parallel and perpendicular to a line connecting the aggregate mass centers.

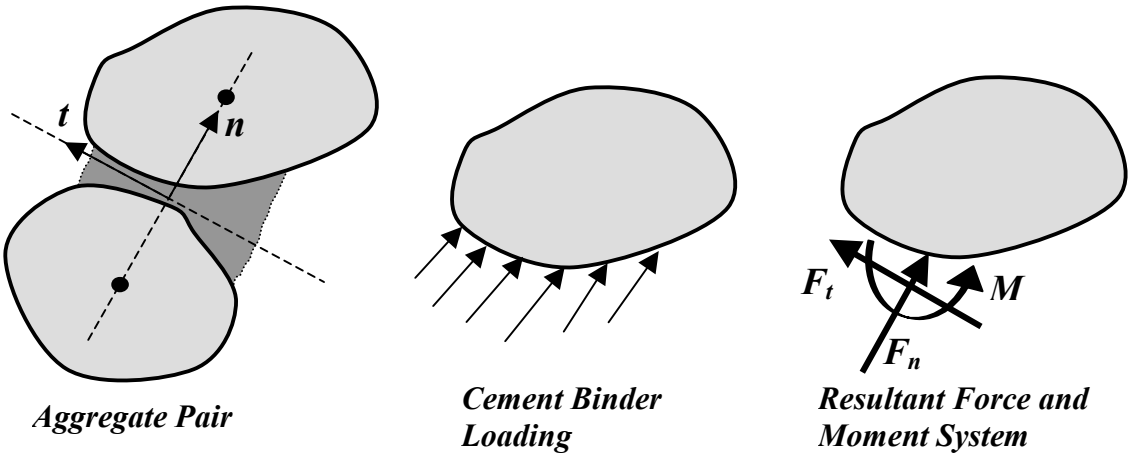

FIGURE 2 Interparticle loading between typical aggregate pairs.

This concept suggests the use of a finite element model to simulate this interparticle load transfer using a frame-type of element. Such a modeling scheme would then replace the cemented aggregate system with a network of specially created finite elements connected at the aggregate mass centers, as shown in Figure 3.

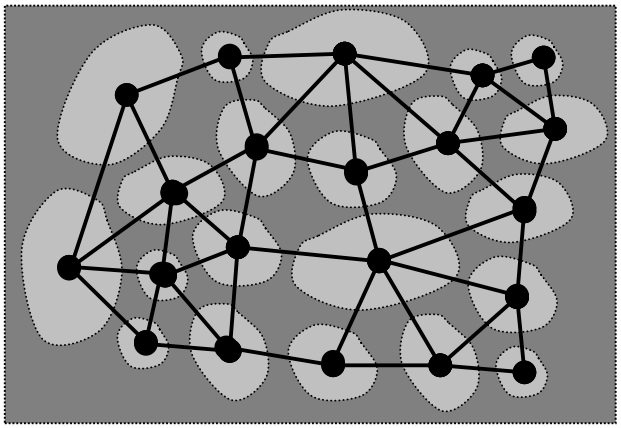

FIGURE 3 Finite element network model.

In order to model the inter-particle load transfer behavior some simplifying assumptions must be made about allowable aggregate shape and the binder geometry. Aggregate geometry has been studied for many years, and recently some work has been conducted on quantifying such geometrical properties, Zhu and Nodes (15), Buchanan (30), Maerz and Lusher (31), Masad, et.al. (32), and Ketcham and Shashidhar (33). Issues related to particle size, shape, angularity and texture have been proposed; however, for the present modeling only size and shape will be considered. In general, asphalt concrete contains aggregate of very irregular geometry as shown in Figure 4(a). Our approach is to allow variable size and shape using a simple elliptical aggregate model as represented in Figure 4(b).

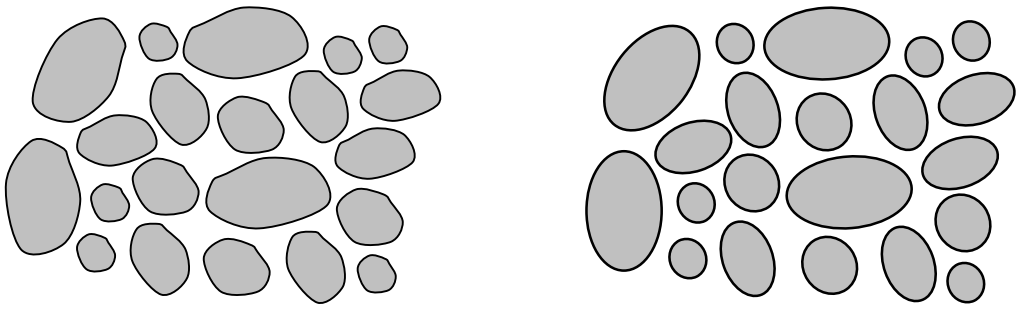

(a) Typical Asphalt Material (b) Model Asphalt System

FIGURE 4 Asphalt aggregate modeling.

Using this scheme, a typical model aggregate pair is shown in Figure 5. In order to construct the various geometrical properties, each idealized elliptical aggregate is characterized by shape measures a_i and b_i, and location and orientation with respect to a global coordinate system. The finite element lies along the *branch vector* defined as the line connecting particle mass centers. The effective binder area is defined as a strip of cementation material parallel to the branch vector as shown. By varying the cementation widths w_1 and w_2, different amounts and distributions of binder can be created within the numerical model.

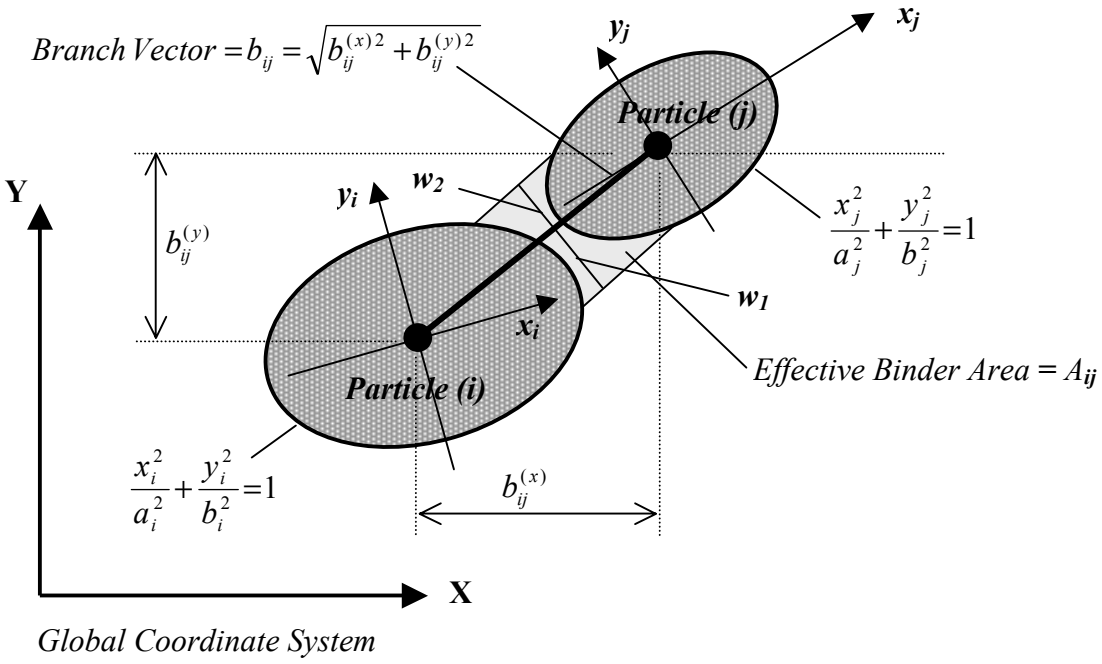

FIGURE 5 Idealized aggregate geometry.

3. FINITE ELEMENT AGGREGATE/BINDER MODEL

We propose to model the interparticle load transfer by using a specially developed frame-type finite element. In order to determine the stiffness properties of the proposed microstructural finite element, consider the element shown in Figure 6. Nodal displacements and rotations correspond to the aggregate mass center motions.

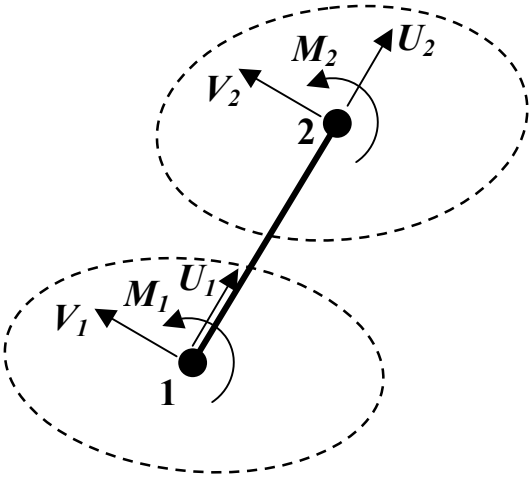

FIGURE 6 Finite element model.

The element has three degrees of freedom at each of the two nodes, and would therefore have the following element equation for the chosen coordinate system,

$$\begin{bmatrix} K_{11} & K_{12} & K_{13} & K_{14} & K_{15} & K_{16} \\ . & K_{22} & K_{23} & K_{24} & K_{25} & K_{26} \\ . & . & K_{33} & K_{34} & K_{35} & K_{36} \\ . & . & . & K_{44} & K_{45} & K_{46} \\ . & . & . & . & K_{55} & K_{56} \\ . & . & . & . & . & K_{66} \end{bmatrix} \begin{Bmatrix} U_1 \\ V_1 \\ \theta_1 \\ U_2 \\ V_2 \\ \theta_2 \end{Bmatrix} = \begin{Bmatrix} F_{n1} \\ F_{t1} \\ M_1 \\ F_{n2} \\ F_{t2} \\ M_2 \end{Bmatrix} \tag{1}$$

For a usual frame element, the various stiffness terms K_{ij} are determined using standard uniaxial bar and Euler-Bernouli or Timoshenko beam theory. However, for our particular application, the asphalt cement cannot be modeled by simple bar or beam action. A more complete stress analysis within the binder material is need, and this can be determined from an approximate elasticity solution originally developed by Dvorkin et.al. (11). This work provides a simple

analytical solution for the stress distribution in a cement layer between two particles. We use the special case where the particle material stiffness is much greater than that of the cement layer, and thus the particles are assumed to be rigid. Dvorkin has shown that effects of non-uniform cement thickness are generally negligible, and so we will use the analytical solution for the uniform cementation case. Dvorkin's two-dimensional model is based on the geometry shown in Figure 7 (uniform cement thickness case). Note that since we are allowing arbitrary non-symmetric cementation (see Figure 5), the finite element will not necessarily pass through the center of the binder material, i.e. . $w = w_1 + w_2$, but $w_1 \neq w_2 \neq w/2$, and an eccentricity variable may be defined by $e = (w_2 - w_1)/2$.

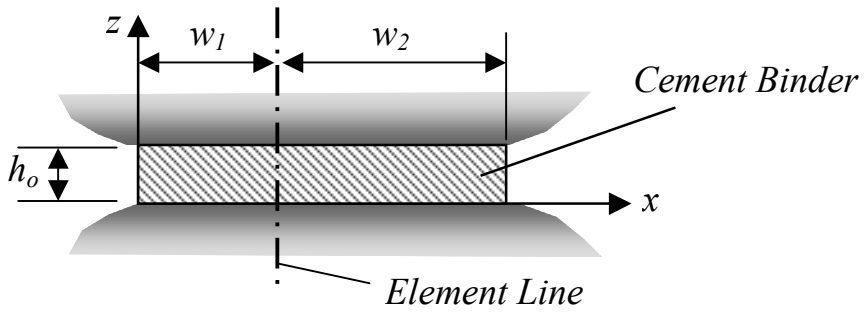

FIGURE 7 Cement layer between two particles.

The stresses σ_x, σ_z and τ_{xz} within the cementation layer can be calculated for particular relative particle motion cases as shown in Figure 8. These stresses can then be integrated to determine the total load transfer within the cement binder.

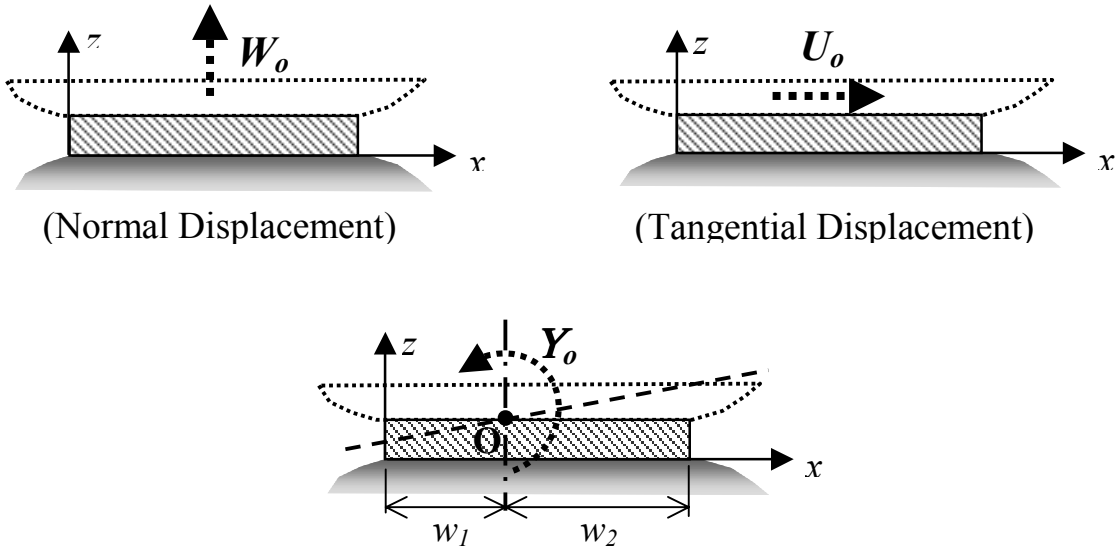

(Normal Displacement) (Tangential Displacement)

(Rotational Displacement @ Point O)

FIGURE 8 Normal, tangential and rotational inter-particle motions.

Resultant force calculations for the cases of normal, tangential and rotational particle motions are given by equations (2), (3) and (4), respectively.

$$F_n = \int_0^w \sigma_z dx = (\lambda + 2\mu)\frac{W_0 w}{h_0}$$
$$F_t = \int_0^w \tau_{xz} dx = 0 \qquad (2)$$
$$M_o = \int_0^w \sigma_z (x - w_1) dx = \frac{1}{2}\sigma_z \left(w_2^2 - w_1^2\right) = (\lambda + 2\mu)\frac{W_0 we}{h_0}$$

$$F_n = \int_0^w \sigma_z dx = 0$$
$$F_t = \int_0^w \tau_{xz} dx = \mu \frac{U_0 w}{h_0} \qquad (3)$$

$$F_n = \int_0^w \sigma_z dx = (\lambda + 2\mu)\frac{\theta_0}{h_0}\int_0^w (x - w_1) dx = (\lambda + 2\mu)\frac{\theta_0 we}{h_0}$$
$$F_t = \int_0^w \tau_{xz} dx = \mu w\left(\frac{h_0 c}{k^2} + \theta_0\right) \qquad (4)$$
$$M_o = \int_0^w \sigma_z (x - w_1) dx = (\lambda + 2\mu)\frac{\theta_0}{h_0}\int_0^w (x - w_1)^2 dx = (\lambda + 2\mu)\frac{\theta_0 w}{3h_0}\left(w_2^2 - w_1 w_2 + w_1^2\right)$$

Using relations (2), (3) and (4) the various stiffness terms K_{ij} in relation (1) can be determined employing the direct stiffness method by making special choices of the nodal displacement vector. The final result is given by

$$[K] = \begin{bmatrix} K_{nn} & 0 & K_{nn}e & -K_{nn} & 0 & -K_{nn}e \\ 0 & K_{tt} & K_{tt}r_1 & 0 & -K_{tt} & K_{tt}r_2 \\ K_{nn}e & K_{tt}r_1 & K_{tt}r_1^2 + \frac{K_{nn}}{3}\left(w_2^2 - w_1w_2 + w_1^2\right) & -K_{nn}e & -K_{tt}r_1 & K_{tt}r_1r_2 - \frac{K_{nn}}{3}\left(w_2^2 - w_1w_2 + w_1^2\right) \\ -K_{nn} & 0 & -K_{nn}e & K_{nn} & 0 & K_{nn}e \\ 0 & -K_{tt} & -K_{tt}r_1 & 0 & K_{tt} & -K_{tt}r_2 \\ -K_{nn}e & K_{tt}r_2 & K_{tt}r_1r_2 - \frac{K_{nn}}{3}\left(w_2^2 - w_1w_2 + w_1^2\right) & K_{nn}e & -K_{tt}r_2 & K_{tt}r_2^2 + \frac{K_{nn}}{3}\left(w_2^2 - w_1w_2 + w_1^2\right) \end{bmatrix} \quad (5)$$

where $K_{nn} = (\lambda+2\mu)w/h_o$, $K_{tt} = \mu w/h_o$, and r_1 and r_2 are the radial dimensions from each aggregate center to the cementation boundary.

4. COMPUTER CODES

As mentioned the purpose of the research was to develop a numerical simulation model, which could predict the two-dimensional behavior of asphalt materials using micromechanical physics. The end result of this work was the creation of computer codes, which implement particular theoretical and analytical formulations. In particular our software development involved the creation of an *asphalt material generating code* and a *finite element simulation code.* The generating code creates idealized materials, which are input into the simulation code to conduct *numerical experiments*. Each of these codes will now be discussed in detail.

4.1 Asphalt Material Generating Code (AMGEN)

In order to simulate the micromechanical behavior of asphalt materials, it is first necessary to create particular idealized asphalt materials. These idealized material models must contain appropriate microstructural geometry such as the size, shape and distribution of the

aggregates, binder and voids. This internal microstructure or *fabric* must be controllable by the software and should allow the user to create a variety of asphalt materials commonly used in pavement applications. With this in mind, we developed the ***A**sphalt **M**aterial **Gen**erator* (AMGEN) code, which was written using MATLAB software. The code has the following general features:

- creates and spatially distributes aggregate particles of circular or elliptical shape
- particle shapes and distributions can be regular or random
- creates and spatially distributes rectangular strips of binder material between neighboring particles
- can create materials of rectangular or circular domain
- generates model geometric and material property files needed as input to the finite element simulation code

The code may be described by considering the required geometrical data needed to generate the material model. Consider first the typical particle pair shown previously in Figure 5. In order to create aggregate microstructure, the following particle geometry is needed: *mass* center location (x_i, y_i); orientation θ_i; and shape factors (a_i, b_i). Binder microstructure requires the geometrical specification of the cementation widths (w_1, w_2). Further code calculations determine additional binder geometry of thickness h_o , average thickness, and cement area. Particle locations allow the calculation of the branch vectors b_{ij} and these in turn become the elements in the finite element network system. Each two-noded element has several microstructural properties including element and nodal numbering, and an overlap marker (0 or 1) to indicate whether the element link crosses with another element in the model. Note that an overlapping element would have a higher overall stiffness property. The generating code decision to create a binder finite element link is determined by a *proximity parameter*. If the

distance between a particle pair (branch vector) exceeds this proximity criterion, the interaction is to be neglected and no element is created for this particular aggregate pair. The basic geometry is developed from user selection of the following: material domain (rectangular or circular); particle type(s); and particle orientation. AMGEN further calculates the total areas of the aggregates, binder and void space, and determines the average material porosity.

Examples of several model materials that have been generated by AMGEN are shown in Figures 9-14. For these particular cases, the particles were distributed evenly along the domain perimeter and particle orientation was randomly specified from 0 to 2π. Aggregates were chosen randomly from a set of four different particle types described by the following major and minor axes dimensions: {(6.0, 5.2) mm, (5.2, 4.5) mm, (6.0, 5.0) mm, (5.5, 5.5) mm}. Figure 9 shows an idealized model material of rectangular shape with specific dimensions of 75mm x 75mm. This model contains 36 aggregate particles, and the cementation is distributed in such a fashion as to create 110 elements of which 25 pairs are of overlapping type. The model material's porosity, 1 - (aggregate + cementation area)/(total area) equals 16%.

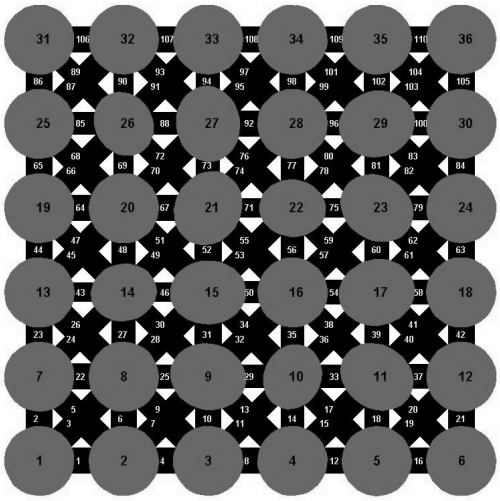

FIGURE 9 Typical rectangular generated material model with 36 aggregates.

Figure 10 shows another rectangular material model with 400 particles. This model has a total 1482 elements (361 overlapping pairs) and has a porosity of 15.4%.

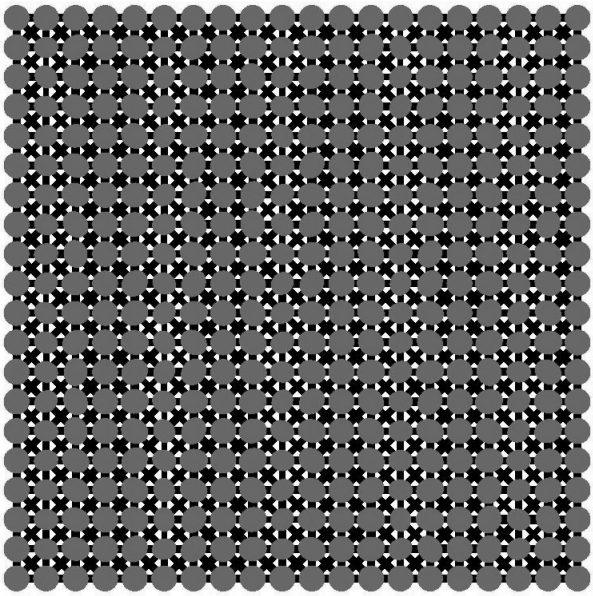

FIGURE 10 Regular rectangular model with 400 aggregates.

The final rectangular model is shown in Figure 11, and this generated system has a total of 1681 particles and 6480 elements.

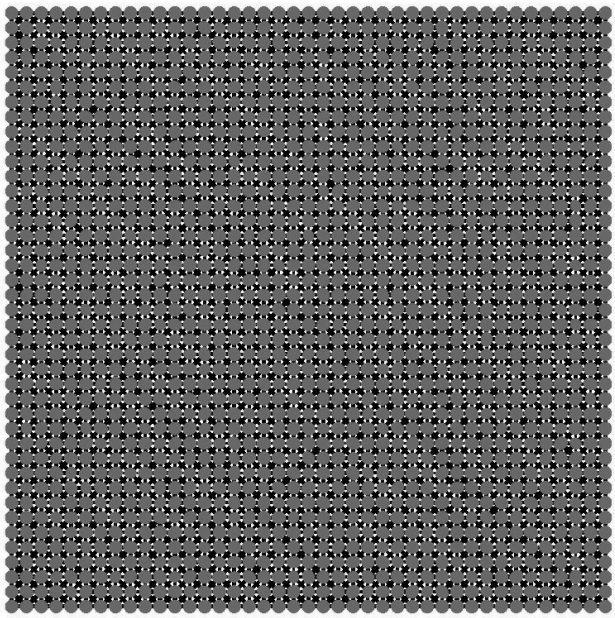

FIGURE 11 Regular rectangular model with 1681 aggregates.

Models of circular domain are shown in Figures 12, 13 and 14. The model in Figure 12 contains 39 particles and 108 elements, while Figures 13 and 14 show material models with 491 and 1321 particles, respectively. Complete details on the model material geometry are given the Table 1.

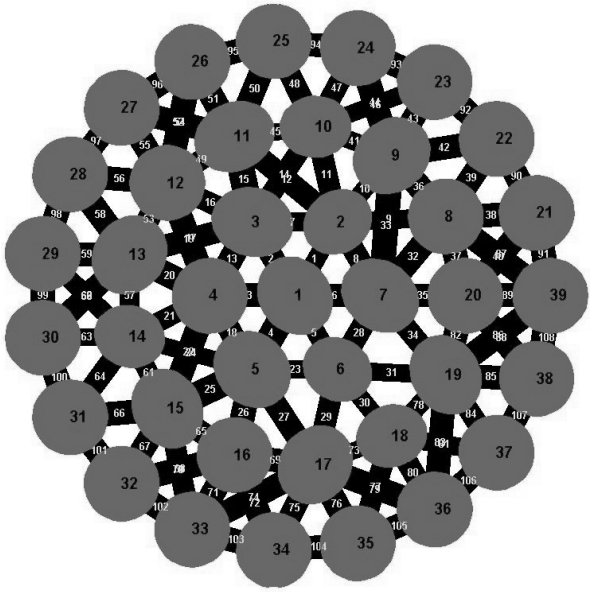

FIGURE 12 Typical model of circular domain with 39 aggregates.

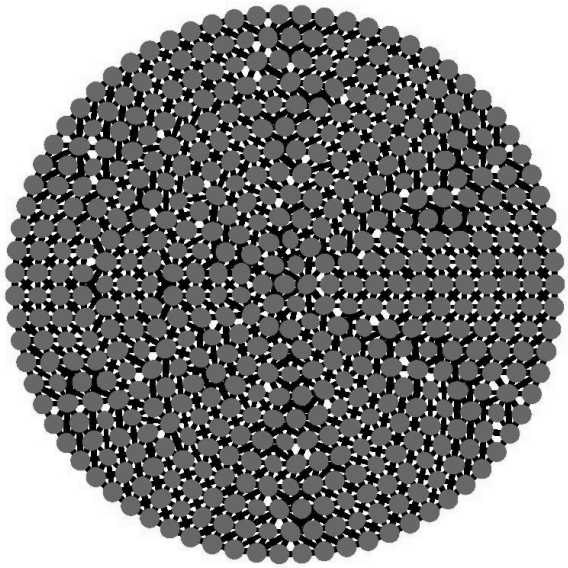

FIGURE 13 Model material of circular domain with 491 aggregates.

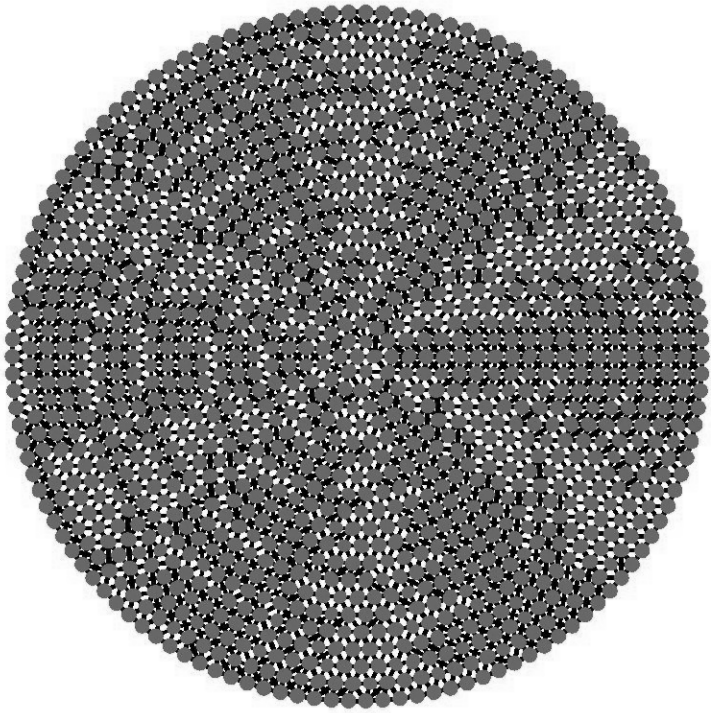

FIGURE 14 Model material of circular domain with 1321 aggregates.

TABLE 1 Model Material Parameters

Model	Domain Dimensions	Number of Particles	Number of Elements	Number of Overlap Element Pairs	Porosity
Figure 9	75x75mm	36	110	25	16.1%
Figure 10	250x250mm	400	1482	361	15.4%
Figure 11	500x500mm	1681	6480	1600	13.2%
Figure 12	R = 43mm	39	108	13	15.8%
Figure 13	R = 155.5mm	491	1851	451	12.6%
Figure 14	R = 255.5mm	1321	4563	729	16.6%

4.2 Finite Element Simulation Code (FEAMS)

In order to incorporate our modeling concepts into a useful simulation tool, a basic two-dimensional, truss-frame finite element computer code is needed. Reddy (34) has given the basics of such a Fortran code for analysis of trusses, and Euler-Bernoulli and Timoshenko frame

structures. Starting with this basic code, we added the special micro-structural frame element and thus developed a new special purpose code for **F**inite **E**lement **As**phalt **M**aterial **S**imulation (***FEAMS***). The new element is based on the developed stiffness matrix given previously in equation (5) using the particulate cementation mechanics developed by Dvorkin (11). A load incrementation scheme was also added to the FEAMS code. A flow chart of the code along with a description of various subroutines are given in Figure 15. The *preprocessor unit* consists of reading input data, generating the finite element mesh and printing data and mesh information. The *processor unit* includes: construction of element matrices; assembly of element equations; imposition of boundary conditions; and solution of system equations for nodal displacements. In the *postprocessor section*, the displacement solution is computed by interpolation at points other than nodes, force values are derived from the displacement solution, and the solution is outputted in desired format. The code subrountines are described as follows:

ECHO: Read the input data and write the input data

ASSMBL: Assemble element equations to the upper-banded form

BONDRY: Impose specified displacement and force boundary conditions

SOLVER: Solve linear algebraic equation to get nodal displacements

TRSFRM: Computer element stiffness matrices and force vectors

SHP1D: Compute the shape function and their derivative

REACTN: Calculate solution at points other than the nodes

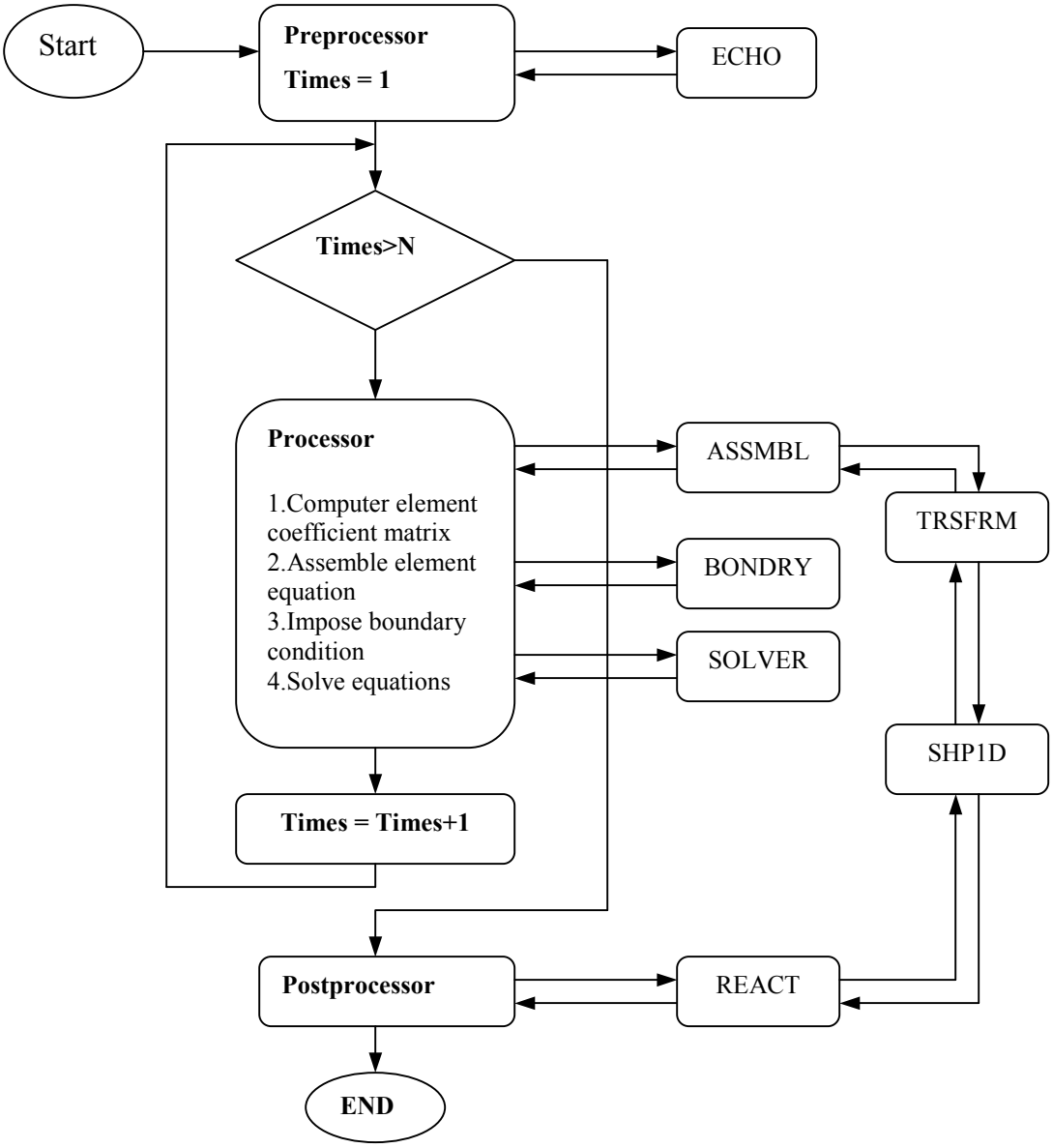

FIGURE 15 Flow chart of the FEAMS code.

5. MODEL VERIFICATION RESULTS

In order to validate the finite element model, several simple numerical verification cases were run. The specific cases included a single element and a 4-cell structure with both symmetric and asymmetric binder distributions. The loadings for each model included three

standard cases for the two-dimensional situation: compression force, shear force and rotation/moment.

5.1 Single Element Verification

In the single element verification, we compare symmetric and asymmetric binder models for the five cases shown in Figure 16. The selected models are chosen to demonstrate the effect of binder properties and eccentricity on the element stiffness behavior. Details of the geometric and mechanical properties for each model are given in Table 2. Each model is to undergo three loading cases of compression, shear (left to right loading) and counter-clockwise moment. The displacement and rotation of node 1 are kept fixed for all loading cases.

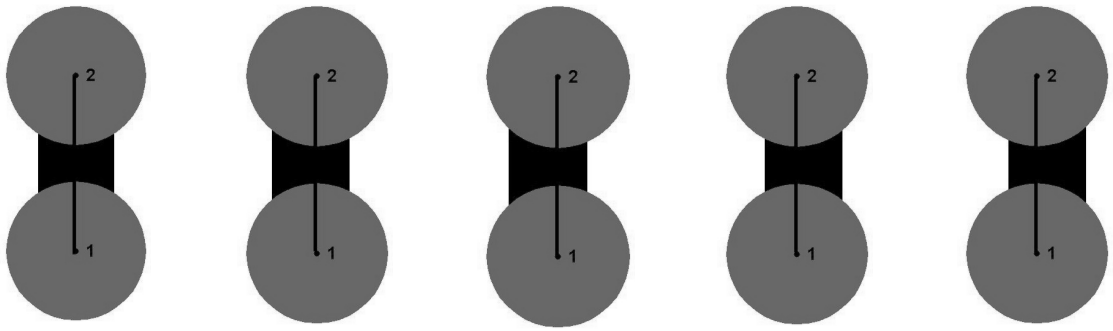

FIGURE 16. Five types of two-node element models.

TABLE 2 Structural Parameters For Single Element Models

Models	Average Thickness $h_0(mm)$	Left Binder Width $w_1(mm)$	Right Binder Width $w_2\ (mm)$	Radius (node 1) $r_1\ (mm)$	Radius (node2) $r_2\ (mm)$	Element Area $S(mm^2)$	Elastic Constants $(E\ MPa, \upsilon)$
Symmetric	3.0	3.0	3.0	5.5	5.5	18.0	(1.0, 0.3)
Asymmetric-A	3.0	3.5	2.5	5.5	5.5	18.0	(1.0, 0.3)
Asymmetric-B	3.0	3.8	2.2	5.5	5.5	18.0	(1.0, 0.3)
Asymmetric-C	3.0	2.5	3.5	5.5	5.5	18.0	(1.0, 0.3)
Asymmetric-D	3.0	2.2	3.8	5.5	5.5	18.0	(1.0, 0.3)

Using the developed finite element code FEAMS, the normal and tangential displacements and rotation at node 2 for each loading case can be determined. Figures 17-19 show the results for a series of loading steps from 0 to 140N.

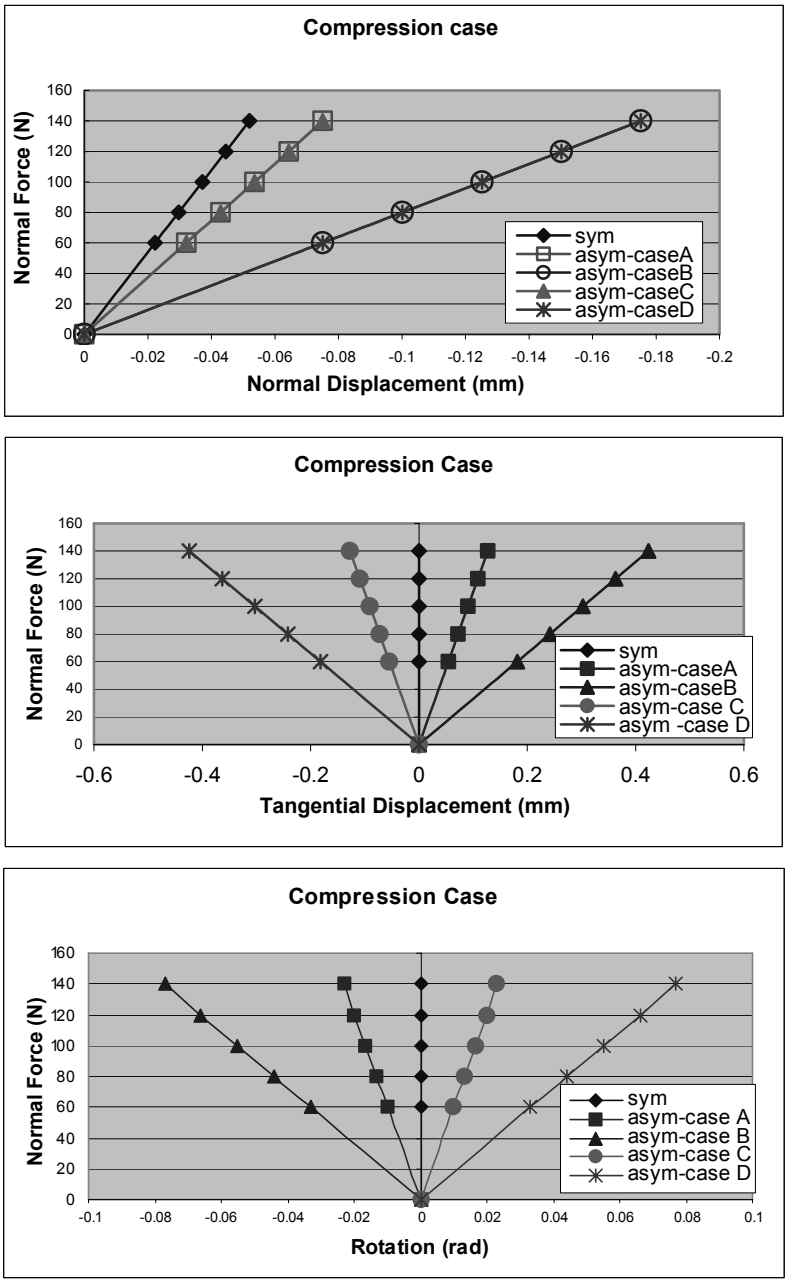

FIGURE 17 Normal, tangential and rotational displacements for the compressional loading case.

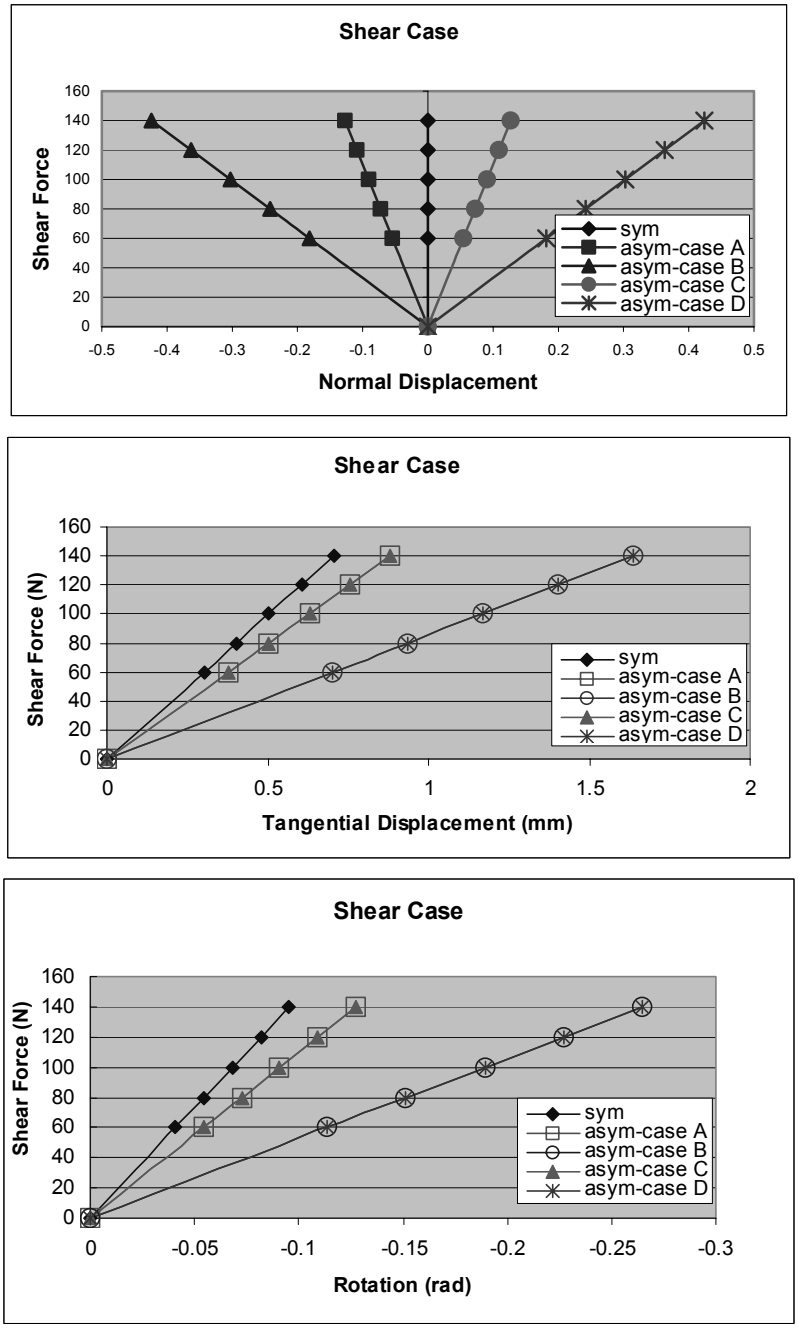

FIGURE 18 Normal, tangential and rotational displacements for the shear loading case.

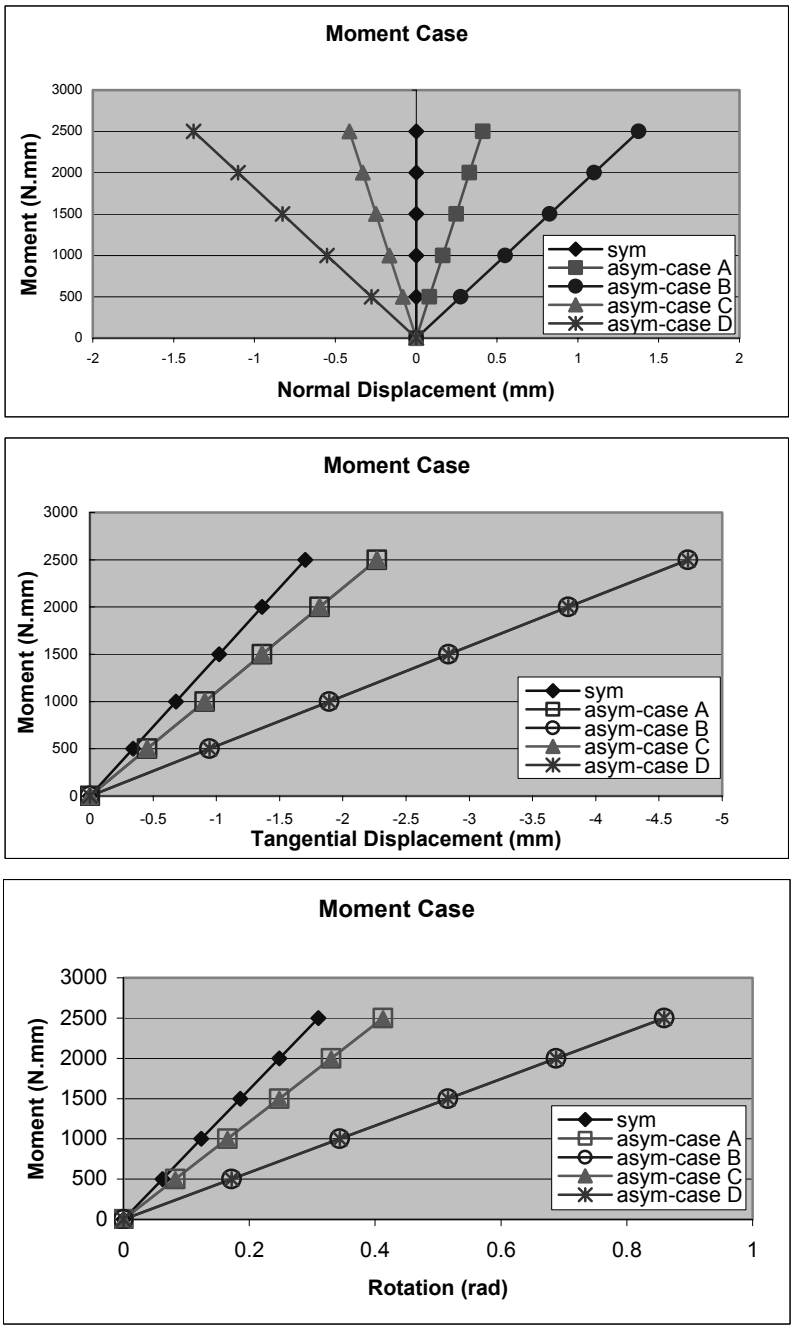

FIGURE 19 Normal, tangential and rotational displacements for the moment loading case.

For the normal loading case, Figure 17 illustrates consistent and symmetric nodal (particle) displacements and rotations. Compressional and shear loading cases for the two-particle problem were independently analyzed using a commercial finite element code (ANSYS), and the

results compared within 4-6%. The increase in displacements with cementation asymmetry has also been verified by independent ANSYS finite element analysis.

4-Cell Verification

In order to verify the behavior of a simple cemented aggregate group, a 4-cell (4-aggregate) microstructure was selected as shown in Figure 20. As in the previous section, both symmetric and asymmetric binder distributions are considered. Each model consists of four elements, and no cross or diagonal elements have been used. Table 3 provides additional specifics on the model data.

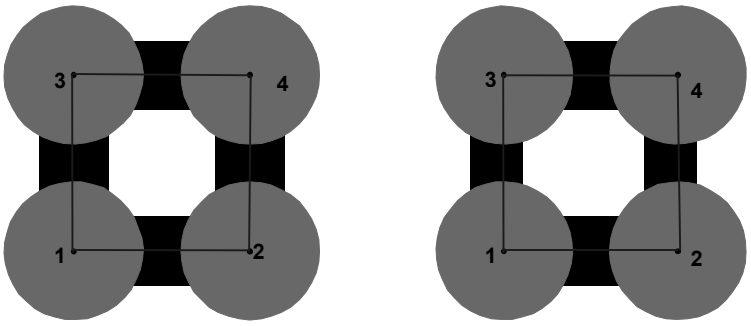

(Symmetric Cemented Cell) (Asymmetric Vertical Binder Cell)

FIGURE 20 Two 4-cell cemented aggregate model structures.

TABLE 3 Structural Parameters For 4-Cell Models

Models	Average Thickness $h_0(mm)$	Left Width $w_1(mm)$	Right Width $w_2\ (mm)$	Radius (node 1) $r_1\ (mm)$	Radius (node2) $r_2\ (mm)$	Element Area $S(mm^2)$	Elastic Constants $(E(MPa), \upsilon)$
Symmetric	3.0	2.5	2.5	5.5	5.5	15.0	(1.0, 0.3)
Asymmetric	3.0	3.0	2.0	5.5	5.5	15.0	(1.0, 0.3)

For this model, node 1 is fixed in the horizontal and vertical, while node 2 is fixed in the vertical. As in the previous example, three loading cases of compression, shear and moment are to be investigated as shown in Figure 21.

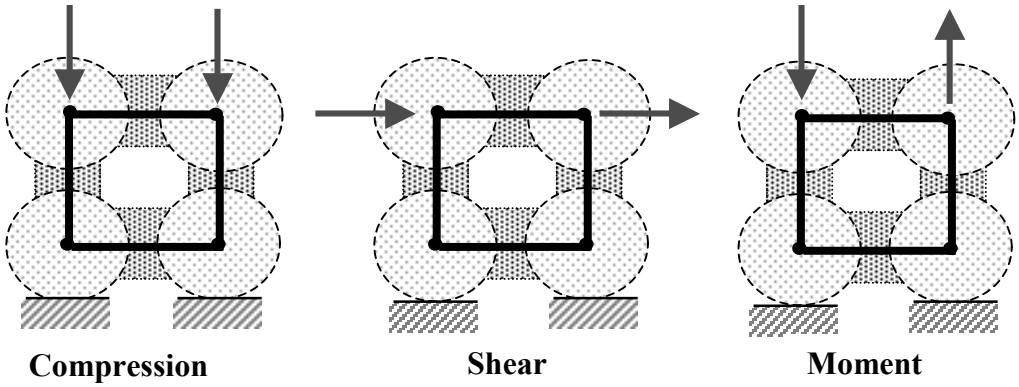

FIGURE 21 Loading cases for the 4-cell model.

Using the FEAMS simulation code, the normal, tangential and rotational displacements associated with nodes 3 and 4 are calculated for a series of loading steps from 0 to 140N. These results are summarized in Figures 22-24.

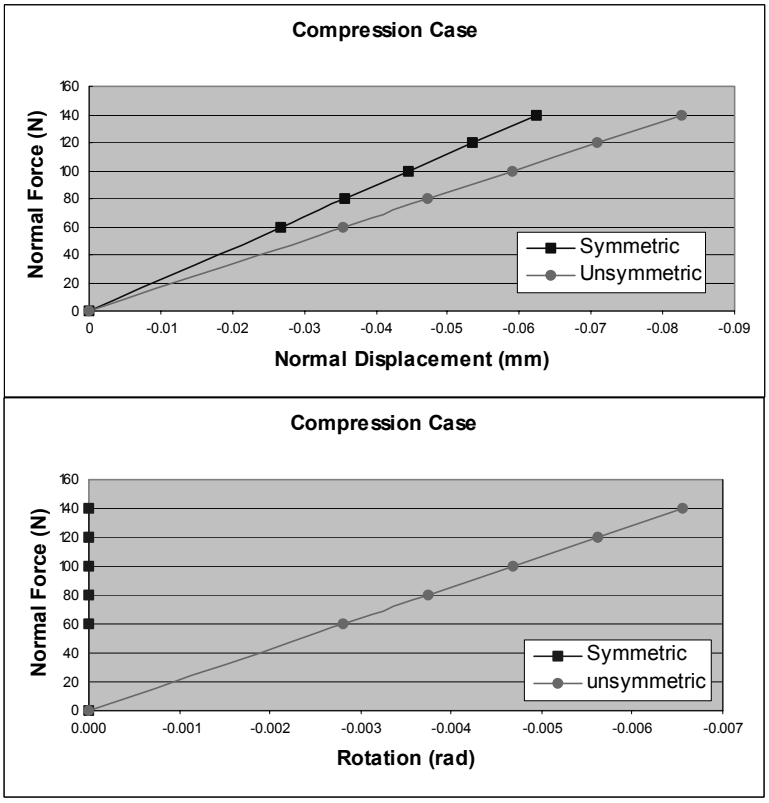

FIGURE 22 Normal and rotational displacements for the compressional loading case.

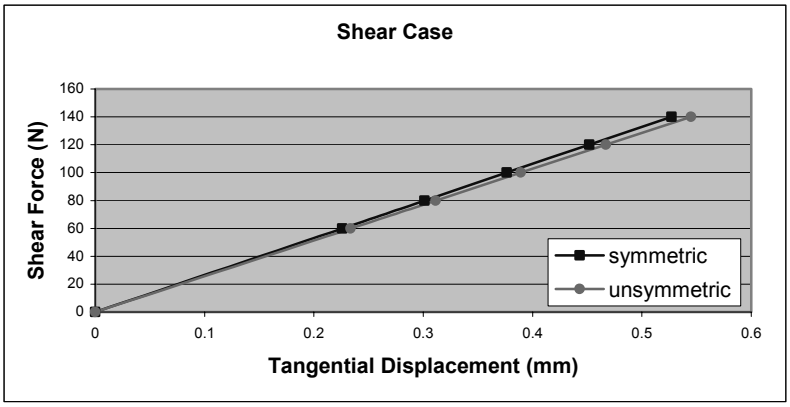

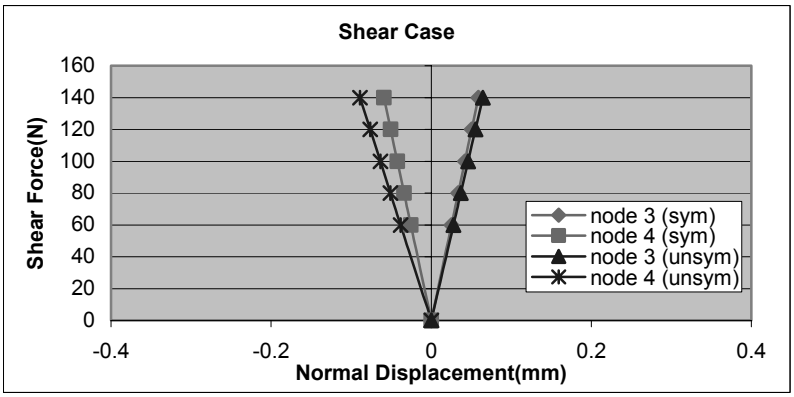

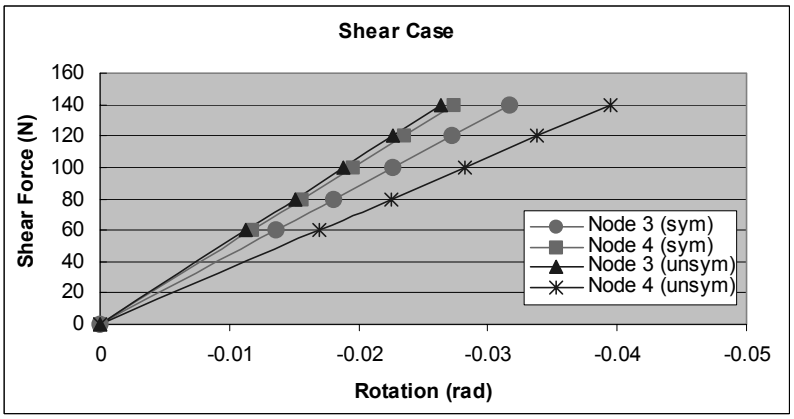

FIGURE 23 Normal, tangential and rotational displacements for the shear loading case.

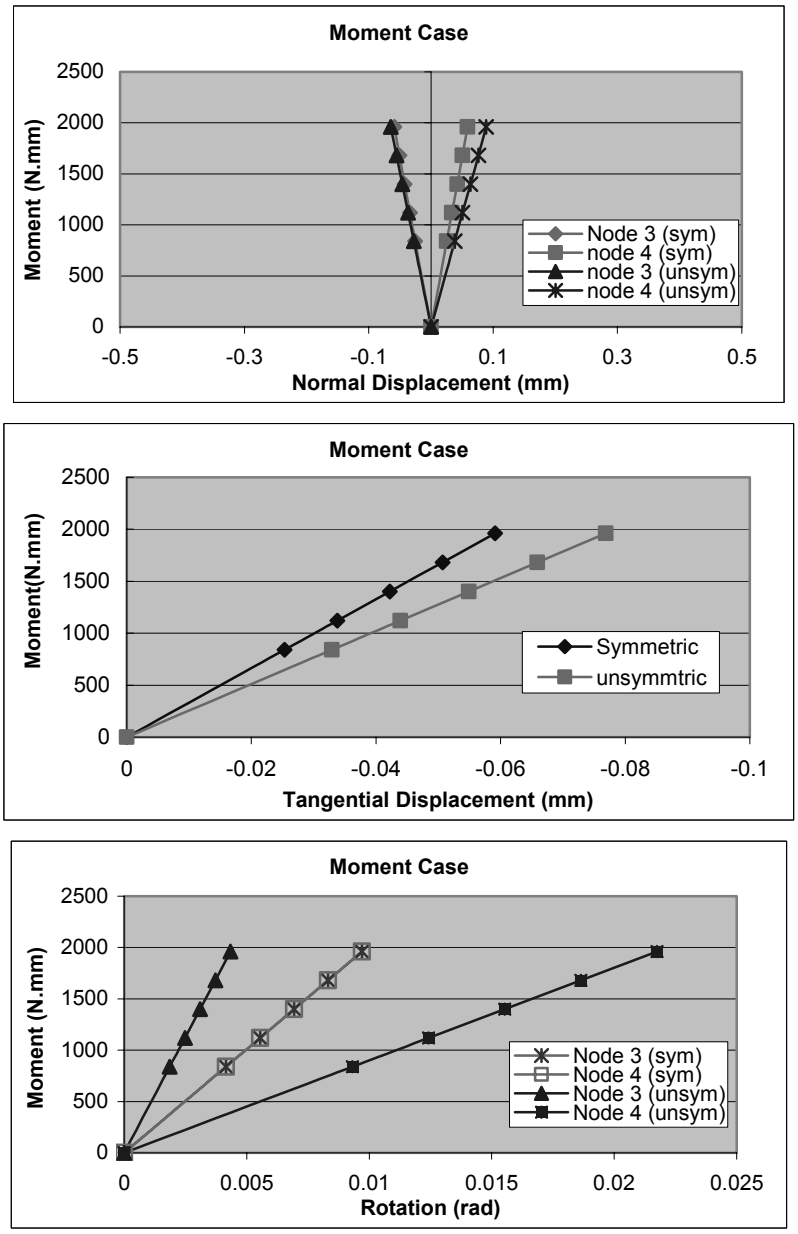

FIGURE 24 Normal, tangential and rotational displacements for the moment loading case.

Figure 22 again shows that asymmetrical cementation produces larger compressional deformation most likely due to the generated rotational motions within the cell structure. For the shear loading case shown in Figure 23, displacement and rotation differences between the symmetric and asymmetric binder geometries seem to be small. The moment loading case

shown in Figure 24 illustrates expected symmetrical normal displacement behaviors; however, the rotational motions appear to be more complex.

6. COMPRESSION AND INDIRECT TENSION SIMULATIONS

The developed modeling has been applied to two common ASTM laboratory tests; i.e. the compression and indirect tension tests. Each test provides a simple method to allow finite element comparisons to be made with standard test data.

6.1 Compression Test Simulation

The geometry of the compression test is shown in Figure 25. Because of the cylindrical symmetry of the specimen and loading, a planar rectangular simulation domain can be taken from the test specimen as shown. This rectangular region would then be appropriate for use with our two-dimensional simulation code, and the simulation information would provide the mechanical response of the specimen under axisymmetric conditions.

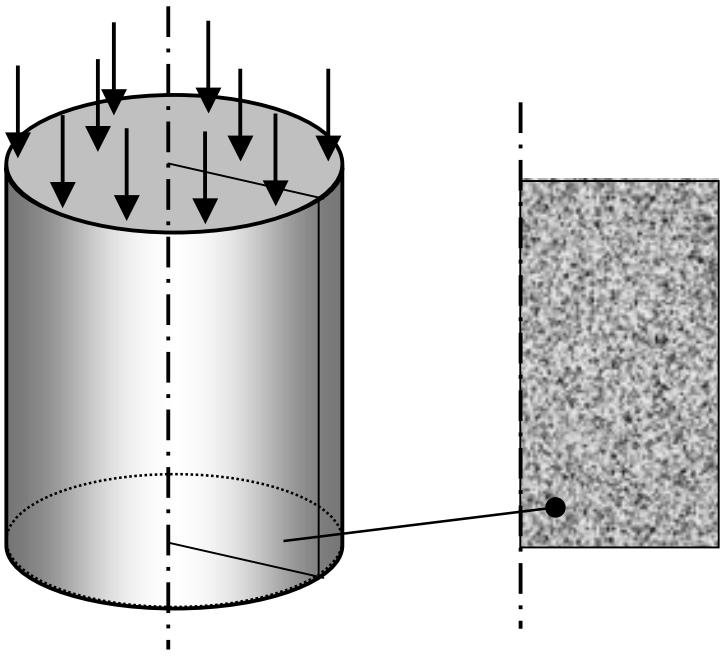

(Test Specimen) (Simulation Domain)

FIGURE 25 Compression test geometry.

The boundary conditions for these simulations are:

- left edge: symmetry conditions of zero horizontal displacement and vertical traction
- right edge: zero forces
- top edge: prescribed loading
- bottom edge: zero vertical displacement and horizontal traction

Three different numerical simulations have been conducted of this test for specimens with a nominal diameter and height of 100mm (4in). For all cases, the cementation width distribution was of uniform value of 1/4 the particle diameter. No stiffness modification was made for overlapping elements. Figure 26 shows a model geometry for a case with 45 equal-sized circular aggregates distributed in a uniform manner in rows and columns. Numerical results of the particle displacements (values scaled for visualization) are also shown in Figure 26.

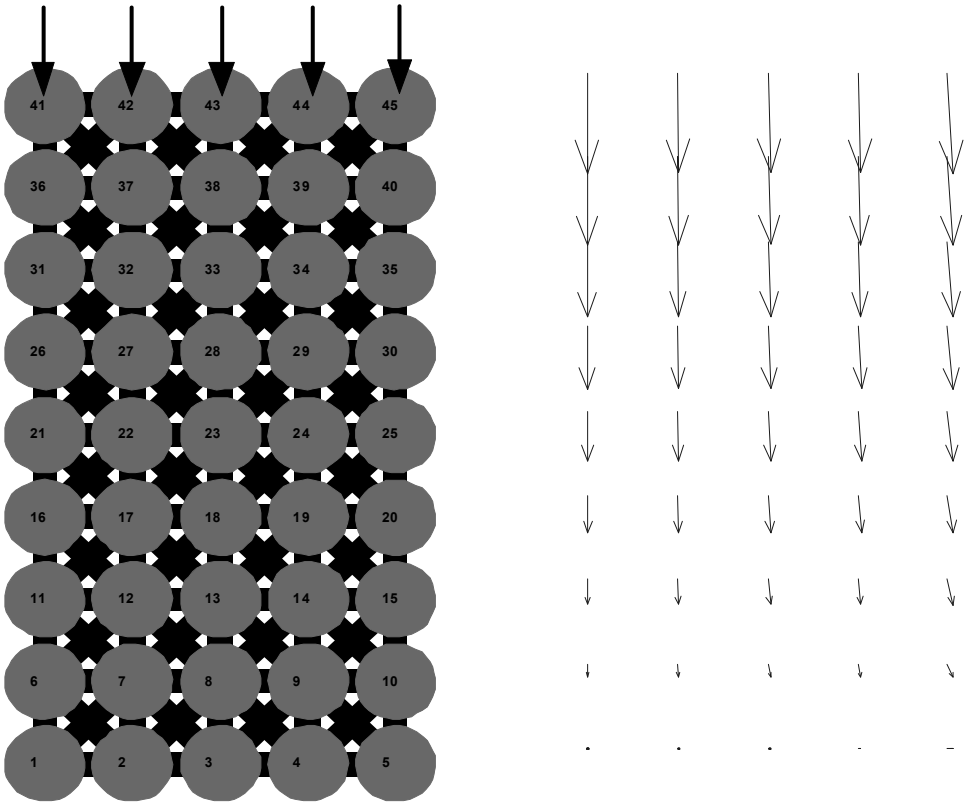

(Material Model) (Aggregate Displacements)

FIGURE 26 Compression test simulation for 45-particle model.

Because of the uniform aggregate size and distribution, the deformation field is quite uniform. The aggregates move down and outward to the right as shown with a maximum vertical displacement along the top edge of 0.187 mm for the applied loading of 500N. Further details on this model are given in Table 4. Another similar model with 153 equal-sized particles are shown in Figure 27. For this case the particle size and spacing was reduced in order to maintaining the same overall nominal specimen dimensions. Numerical results of the particle displacements (values scaled for visualization) are shown in Figure 27. Similar to the previous case, the deformation field is again very uniform with vertical displacements being predominant with a maximum value of 0.29mm along the top edge with a vertical loading of 900N. Additional details on this model are given in Table4.

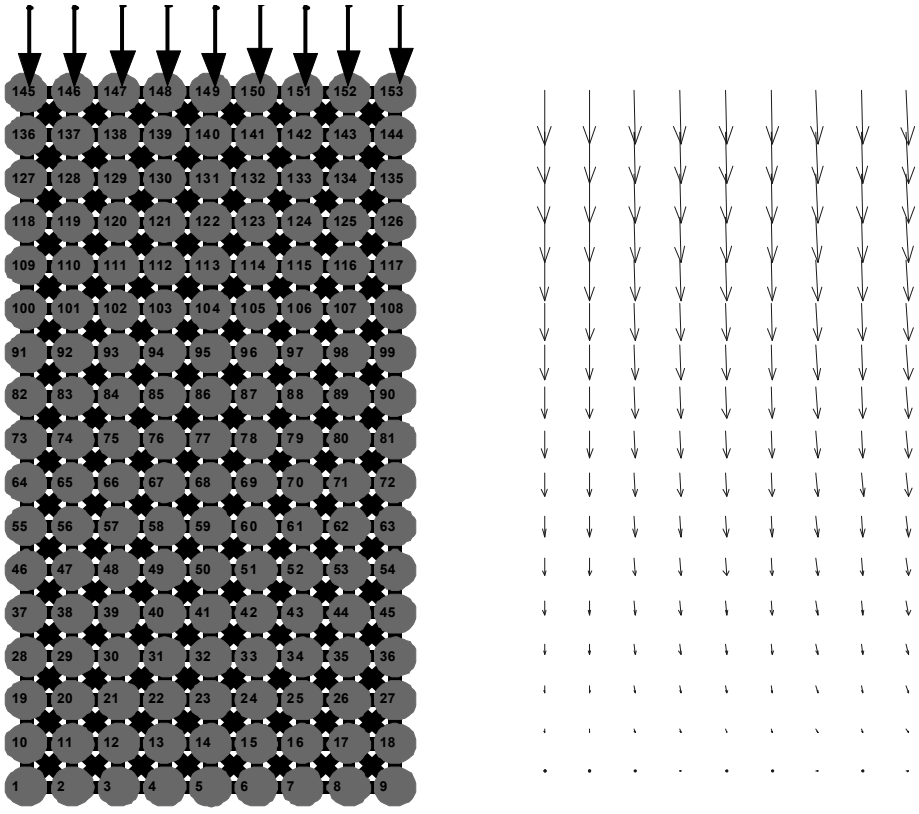

(Material Model) (Aggregate Displacements)

FIGURE 27 Compression test simulation for 153-particle model.

The final numerical simulation of this specimen type modifies the previous case to include 153 aggregates of variable size and shape. Four different aggregate types are randomly used in this model and Table 4 indicates the specific aggregate dimensions used. Figure 28 shows the model geometry for this variable aggregate case along with the corresponding deformation field from the numerical simulation. Although it is not very easy to observe from the figure, the particle displacements are now no longer completely uniform, and we see the local effects of variable microstructure on the deformation field. Again Table 4 provides additional details on this particular model.

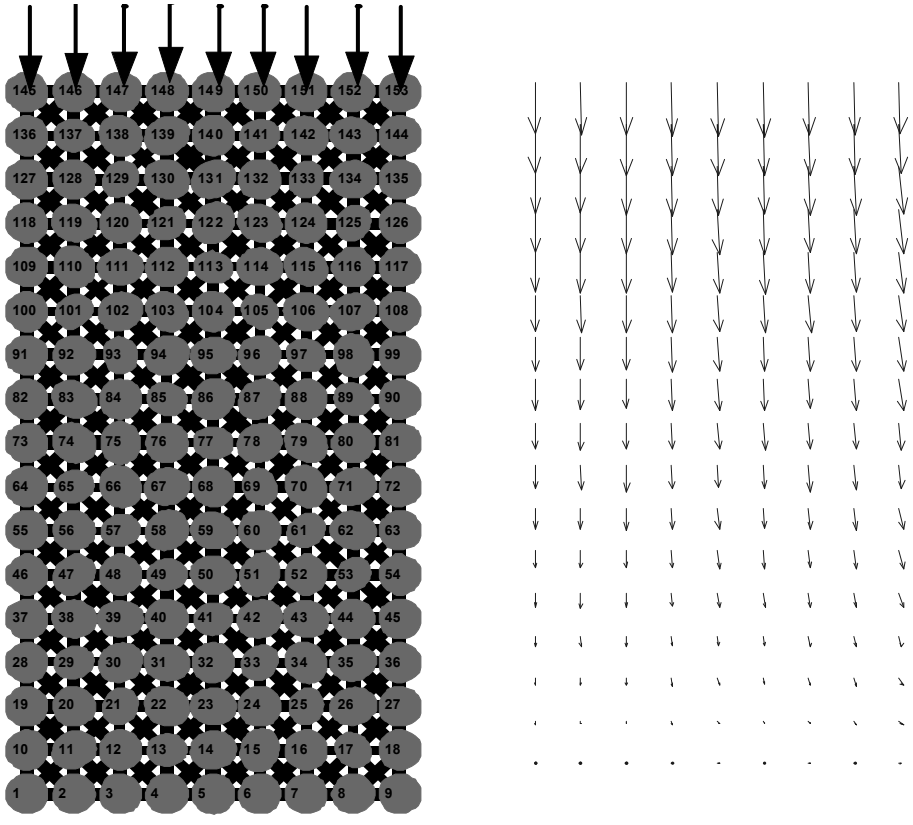

(Material Model) (Aggregate Displacements)

FIGURE 28 Compression test simulation for variable size 153-particle model.

TABLE 4 Properties of Compression Test Model

	Figure 26	Figure 27	Figure 28
Number of Particles	45	153	153
Particle Size, (*a,b*) (mm)	(5.5, 5.5)	(2.75,2.75)	(2.6, 2.2) (3.0, 2.6) (3.0, 2.5) (2.75, 2.75)
Horz. and Vert. Binder Thickness (mm)	1	0.5	0.5
Number of Elements	140	536	536
Number of Overlap Element Pairs	32	128	128
Porosity	13.1%	11.1%	13.5%
Binder Elastic Constants (*E* (Mpa), ν)	(1.0, 0.3)	(1.0, 0.3)	(1.0, 0.3)
Vertical Loading (N)	500	900	900
Max Vertical Displacement (mm)	0.187	0.290	0.392

6.2 Indirect Tension Test Simulation

The indirect tension test (IDT) is used to determine the tensile or splitting strength of bituminous materials, and the typical geometry is shown in Figure 29. A cylindrical specimen is loaded diametrically in compression, and this loading produces a somewhat uniform tension zone in the specimen across the loaded diameter. Normally the specimen thickness is to be kept smaller than the diameter. Again because of uniform loading through the thickness, a two-dimensional circular cross-section may be taken for the numerical simulation domain, as shown.

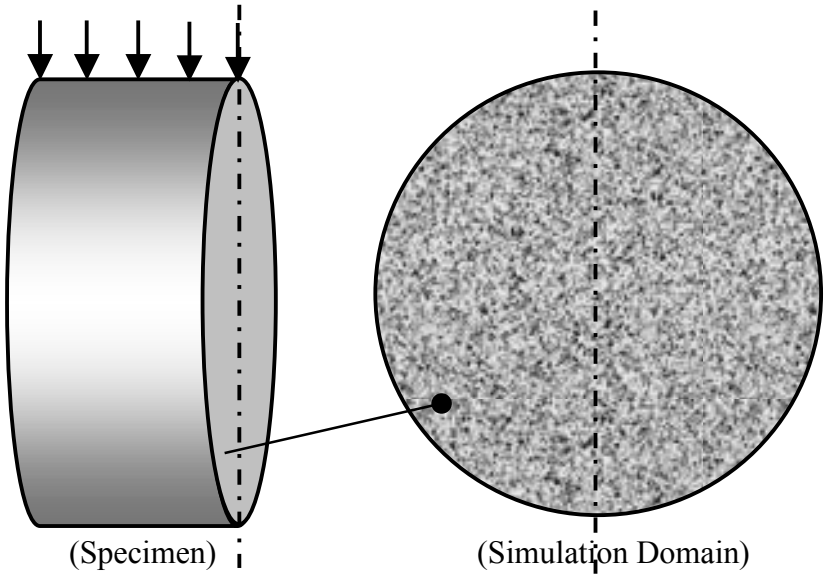

FIGURE 29 Indirect tension test geometry.

Again three different numerical simulations have been conducted on typical indirect tension test specimens with a nominal diameter of 100mm (4in). For all cases, the cementation width distribution was of uniform value of 1/4 the particle diameter. No modification was made for overlapping elements. Boundary conditions fixed the bottom aggregate for both horizontal and vertical displacements while the top particle is constrained only for horizontal motion. Figure 30 shows a simulation with 64 equal-sized circular particles loaded through three aggregates. The corresponding deformation field is also shown in the displacement vector plot.

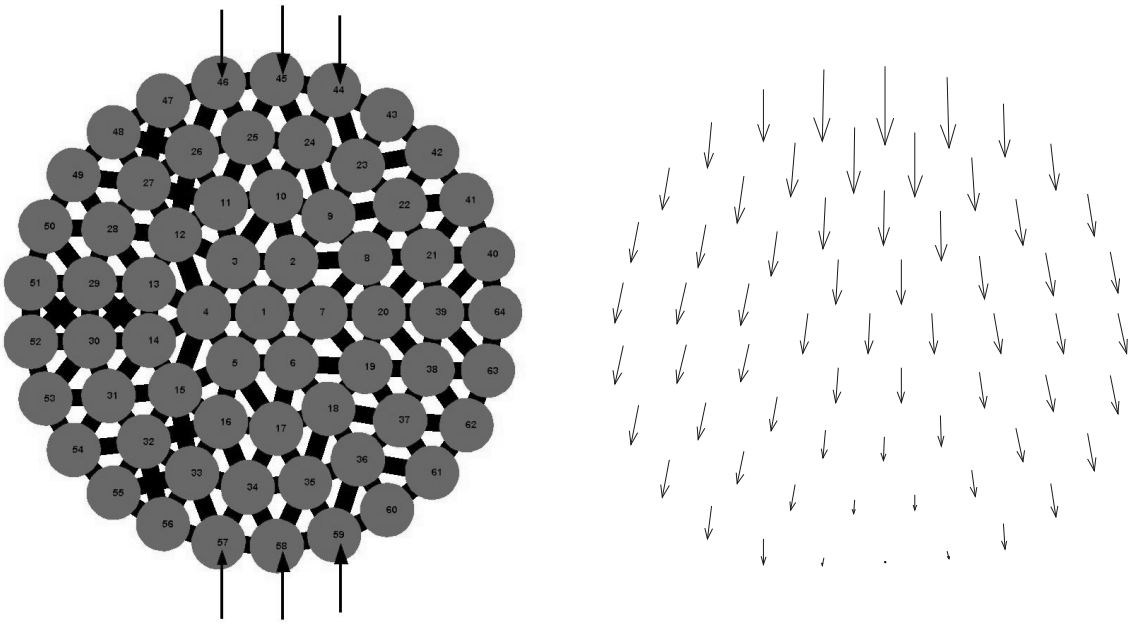

(Material Model) (Aggregate Displacements)

FIGURE 30 Indirect tension test simulation for 64 aggregate model.

For this simulation, we see a predominant vertical deformation pattern with downward aggregate displacements being much larger than the horizontal components. With a total loading of 300N, the maximum vertical displacement was 0.163mm, which occurred directly under the loading on aggregate #45. Further details on this model are provided in Table 5. Another simulation as shown in Figure 31 was run on a model with a larger number of smaller particles. This model had 227 particles of uniform circular shape arranged in a similar distribution pattern as the

previous case. The deformation field is also shown in the figure including vertical, horizontal and total particle displacement plots. Again it is seen that the vertical displacements represent

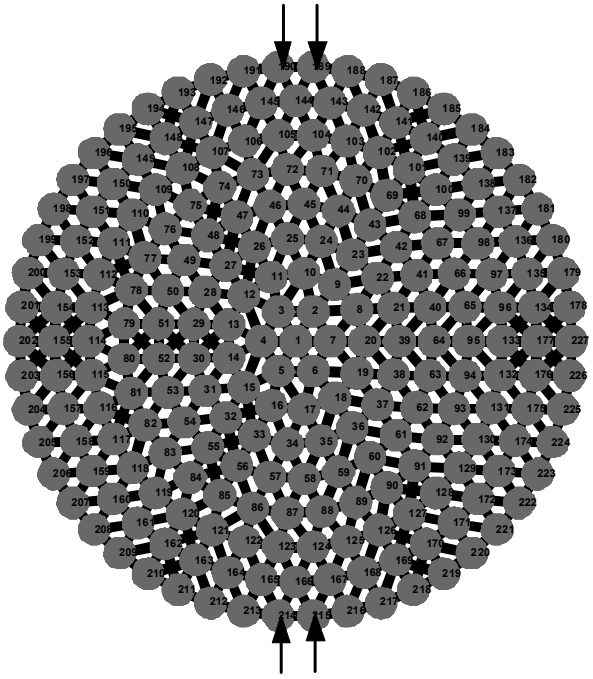

(Material Model)

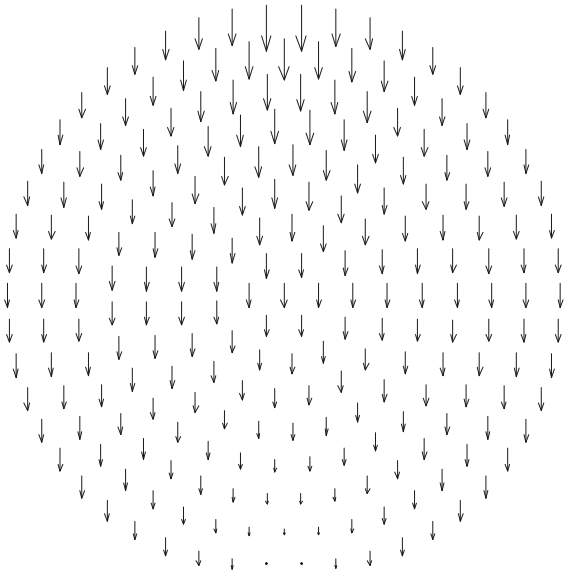

(Vertical Displacements)

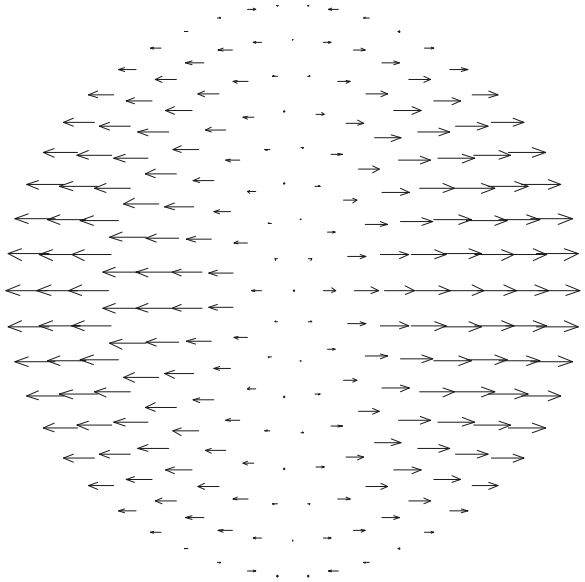

(Horizontal Displacements)

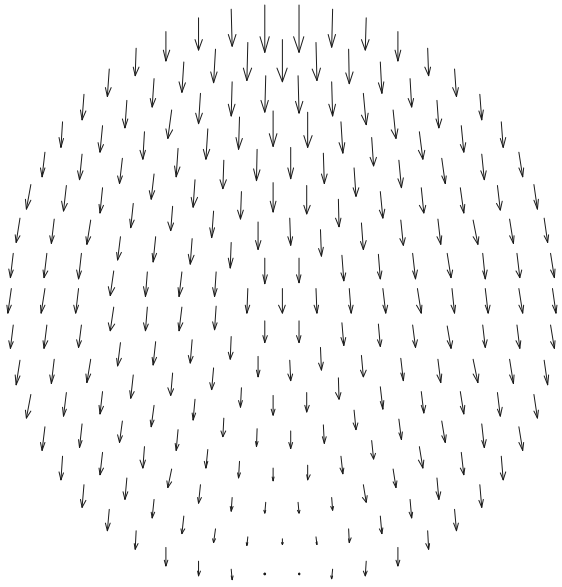

(Total Resultant Displacements)

FIGURE 31 Indirect tension test results for 227 particle model.

the primary deformations of the aggregates in the asphalt model. The horizontal displacement figure illustrates the splitting action of the test specimen with the tendency of deformations to separate the specimen along the vertical centerline. Additional details on this model geometry are given in Table 5. The final IDT simulation is similar to the previous case but with particles of different size and orientation. The 227 aggregates are randomly chosen from a set of four particle types as listed in Table 5. The model and the horizontal displacements are shown in Figure 32. For this variable aggregate case, the displacement field is no longer symmetric. Contrary to the previous case, the horizontal deformation field for this model indicates the tendency for splitting action to occur not directly along the specimen centerline.

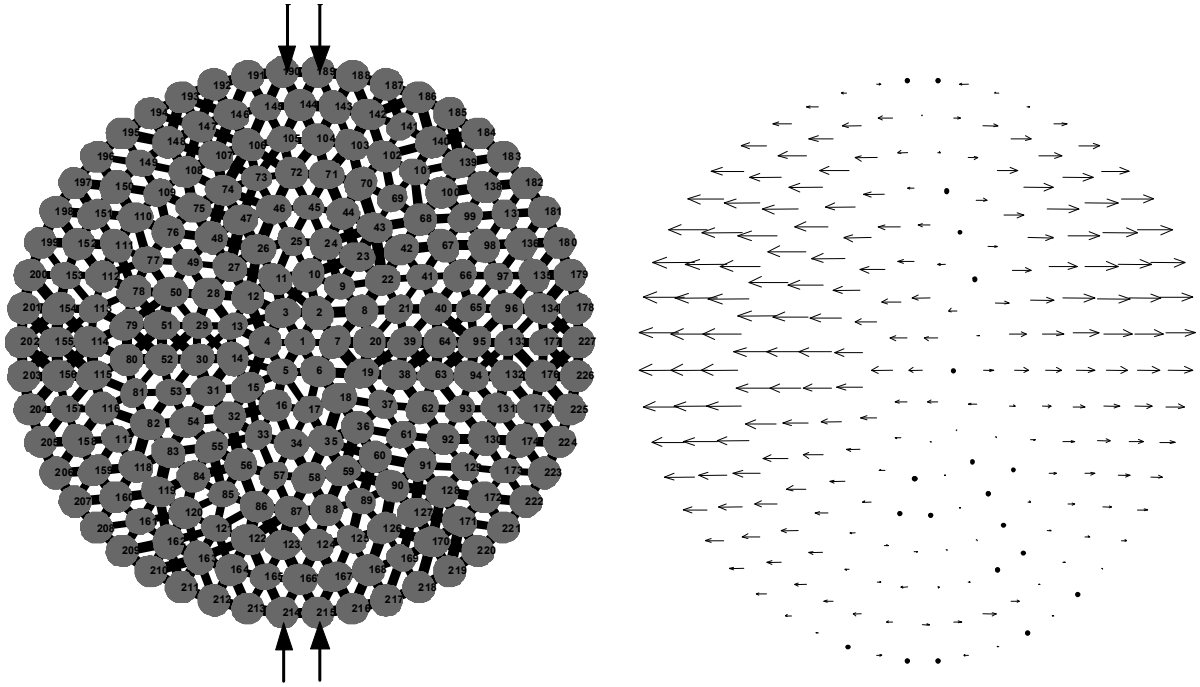

(Material Model) (Horizontal Displacements)

FIGURE 32 Indirect tension test simulation for variable size aggregate model.

TABLE 5 Properties of Indirect Tension Test Model

	Figure 30	Figure 31	Figure 32
Number of Particles	64	227	227
Particle Size, (*a,b*) (mm)	(5.5, 5.5)	(2.75,2.75)	(2.6, 2.2) (3.0, 2.6) (3.0, 2.5) (2.75, 2.75)
Circumferential Binder Thickness (mm)	1	0.5	0.5
Number of Elements	170	657	657
Number of Overlap Element Pairs	6	29	48
Porosity	15.7%	16.5%	17.7%
Binder Elastic Constants (E (Mpa), ν)	(1.0, 0.3)	(1.0, 0.3)	(1.0, 0.3)
Vertical Loading (N)	300	200	200
Max Vertical Displacement (mm)	0.163	0.178	0.184

A comparison of our finite element model results with an actual experimental IDT test has been done. The standard IDT test was conducted on an asphalt sample with properties: Diameter = 101mm (4in), Thickness = 70mm, 6% asphalt content, Aggregate Size Distribution (8% 0.075-2.36mm, 28% 2.36-4.75mm, 25% 4.75-9.5mm, 30% 9.5-12.5mm, 5% 12.5-19mm). Out finite element model used the microstructure geometry shown in Figure 31 with a uniform particle size of 5.5mm, which approximately matched the average aggregate size of the test specimen. The model dimension matched the test specimen size and the binder elastic moduli were E = 1.24MPa and ν = 0.3. Comparisons of the load versus deformation are shown in Figure 33. The experimental data shows initial elastic behavior followed by inelastic yielding and eventual failure. Our modeling results are of course valid only in the elastic region and they match very well with the experimental data. Future model development will incorporate inelastic behaviors and will lead to a capability of simulating the entire load-deflection curve of this and other laboratory tests.

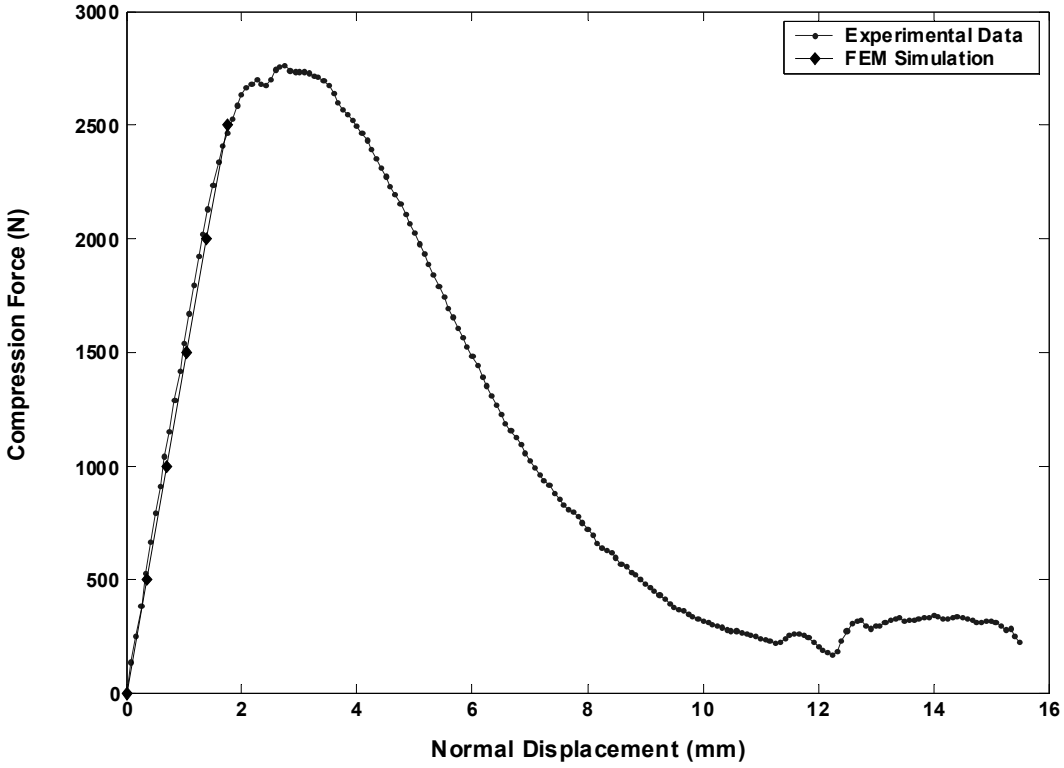

FIGURE 33 Comparison of finite element simulation with experimental IDT test.

7. SUMMARY & CONCLUSIONS

This study has developed a preliminary microstructural finite element model for the two-dimensional simulation of asphalt materials. Asphalt microstructure was incorporated into the model by replacing the aggregate-binder system with an equivalent finite element network that represents the load-carrying behavior between aggregates in the multiphase material. Elements within the network are specially developed from an elasticity solution for cemented particulates proposed by Dvorkin (11). Based on this modeling work, a computer simulation code named FEAMS was created. Our modeling has also developed a material generating code (AMGEN), which can create an aggregate-binder system with varying degrees of microstructure. Currently, AMGEN can create models of rectangular and circular domain with variable aggregate and

binder size, shape, and distribution. AMGEN acts as a pre-processor, and thus creates all the material and geometric data needed by the FEAMS simulation code.

Several comparative verification computer runs have been conducted on single element and 4-cell aggregate structures. Model simulations of standard laboratory experiments including compression and indirect tension tests are also given. Currently, model binder cement distributions were arbitrarily specified; however, more sophisticated distribution schemes based on surface wetting and adhesion are currently under development. Comparison of model predictions with test data for a standard IDT test was made, and the model results match well with the experimental data. The model simulation results are preliminary and are currently limited to two-dimensional, linear elastic conditions. However, these results do indicate that the modeling scheme provides useful comparisons and information, and that with further development the model can be applied to recycled asphalt materials. Various recycling effects related to aging and oxidation can be incorporated into the model by allowing element properties to have more varied elastic, plastic, viscoelastic and damaged behaviors. Further connections with plant recycling processes would require an experimental testing program with model simulations, and it is anticipated that such further studies will begin in the near future.

Future plans for such model development will include the following features:

- non-elastic binder behavior
- non-linear binder behavior including aging, microcracking and damage
- finite deformations
- binder-aggregate separation
- three-dimensional finite element modeling

8. REFERENCES

(1) Schimmoller, V.E, Holtz, K, et.al., Recycled Materials in European Highway Environments: Uses, Technologies and Policies, FHWA/US DOT Report, Presented at 80th TRB Meeting, Washington, D.C., January, 2001.

(2) Kandhal, P.S., Rao, S.S., Watson, D.E. and B. Young, Performance of Recycled Hot Mix Asphalt Mixtures", NCAT Report No. 95-1, 1995.

(3) Brayton, T.E., Lee, K.W., Gress, D. and J. Harrington, Development of Perfomance-Based Mix Design for Cold In-Place Recycling of Asphalt Mixtures, Proc.80th Transportation Research Board Meeting, Washington, D.C., 2001.

(4) Salam, Y.M. and C.L. Monismith, Fracture Characteristics of Asphalt Concrete, Proceedings of the Association of Asphalt Paving Technologists (AAPT), Vol. 41, 1972.

(5) Majidzadeh, K. and Kauffmann, E., Verification of Fracture Mechanics Concepts to Predict Cracking of Flexible Pavements, Research Foundation, Ohio State University, RF 3200, Final Report, 1973.

(6) Majidzadeh, K., Dat, M. and F. Makdisi-Illyas, Application of Fracture Mechanics for Improved Design of Bituminous Concrete, Report No: FHWA-RD-76-92, 1976.

(7) Karakouzian, M. and K. Majidzadeh, Practical Method for Evaluating Fatigue and Fracture Toughness of Paving Materials, AAPT Proceedings, 1978.

(8) Sousa, J. and C.L. Monismith, Dynamic Properties of Asphalt Concrete, Journal of Testing and Evaluation, Vol. 114, No: 4, 1988.

(9) Sulaiman, F. J. and A.F. Stock, The Use of Fracture Mechanics for the Evaluation of Asphalt Mixes, AAPT Proceedings, Vol. 64, 1996.

(10) Venkatram, S., Fracture Toughness and Dynamic Constitutive Characterization of Recycled Asphalt Pavement Binder, Masters Thesis, University of Rhode Island, 1996.

(11) Dvorkin, J., Nur, A., H. Yin, Effective Properties of Cemented Granular Materials, Mech.of Materials, Vol 18, pp 351-366, 1994.

(12) Zhu, H., Chang, C.S. and J.W. Rish, Normal and Tangential Compliance for Conforming Binder Contact I: Elastic Binder, Intl. J. Solids Structures, Vol. 33, pp 4337-4349, 1996.

(13) Zhu, H., Chang, C.S. and J.W. Rish, Normal and Tangential Compliance for Conforming Binder Contact II: Viscoelastic Binder, Intl. J. Solids Structures, Vol. 33, pp 4351-4363, 1996.

(14) Zhu, H., Contact Mechanism Based Asphalt Concrete Modeling, Proc. 12th ASCE Engineering Mechanics Conference, San Diego, May 1988.

(15) Zhu, H. and J.E. Nodes, Contact Based Analysis of Asphalt Pavement with the Effect of Aggregate Angularity, Mech. Of Materials, Vol. 32, pp. 193-202, 2000.

(16) Krishnan, J.M. and C.L. Rao, Mechanics of Air Voids Reduction of Asphalt Concrete Using Mixture Theory, Int. Jour. Eng. Sci., Vol. 38, pp. 1331-1354, 2000.

(17) Rothenburg, L., Bogobowicz, A. and R. Haas, Micromechanical Modeling of Asphalt Concrete in Connection with Pavement Rutting Problems, Proc. 7th Intl. Conf. On Asphalt Pavements, Vol. 1, pp. 230-245, 1992.

(18) Chang, G.K., and N.J. Meegoda, Simulation of the Behavior of Asphalt Concrete Using Discrete Element Method, Proc. 2nd Intl. Conf. On Discrete Element Methods, M.I.T, 1993.

(19) Trent, B.C. and L.G. Margolin, Modeling Fracture in Cemented Granular Materials, ASCE Pub. Fracture Mechanics Applied to Geotechnical Engineering, Proc. ASCE National Convention, Atlanta, 1994.

(20) Buttlar, W.G. and Z. You, Discrete Element Modeling of Asphalt Concrete: A Micro-Fabric Approach, Proc. 80th Transportation Research Board Meeting, Washington, D.C., 2001.

(21) Ullidtz, P., A Study of Failure in Cohesive Particulate Media Using the Discrete Element Method, Proc. 80th Transportation Research Board Meeting, Washington, D.C, 2001.

(22) Sadd, M.H. and J.Y. Gao, The Effect of Particle Damage on Wave Propagation in Granular Materials, *Mechanics of Deformation and Flow of Particulate Materials*, pp 159-173, Ed. C.S. Chang, A. Misra, R.Y. Liang and M. Babic, Proc. McNu Conference, Trans. ASCE, Northwestern Univ., June 1997.

(23) Sadd, M.H., and J.Y. Gao, Contact Micromechanics Modeling of the Acoustic Behavior of Cemented Particulate Marine Sediments, Proc. 12th ASCE Engineering Mechanics Conf., La Jolla, CA, 1998.

(24) Stankowski, T., Numerical Simulation of Progressive Failure in Particle Composites", Ph.D. Thesis, Univserity of Colorado, 1990.

(25) Liao, C.L. and C.S. Chang, A Microstructural Finite Element Model for Granular Solids, Eng. Comp., Vol 9, pp 267-276, 1992.

(26) Bazant, Z.P., Tabbara, M.R, Kazemi, T., and G. Pijaudier-Cabot, Random Particle Simulation of Damage and Fracture in Particulate or Fiber-Reinforced Composites, Damage Mechanics in Engineering Materials, AMD Vol 109, Trans. ASME, 1990.

(27) Sadd, M.H., Qiu, L., Boardman, W., and A. Shukla, Modeling Wave Propagation in Granular Materials Using Elastic Networks", Intl. J. Rock Mechanics & Minning Sci, Vol. 29, p. 61, 1992.

(28) Budhu, M., Ramakrishnan, S. and G. Frantziskonis, Modeling of Granular Materials: A Numerical Model Using Lattices", *Mechanics of Deformation and Flow of Particulate Materials*, Ed. C.S. Chang, A. Misra, R.Y. Liang and M. Babic, Proc. McNu Conference, Trans. ASCE, Northwestern Univ., June 1997.

(29) Mustoe, G.G.W. and D.V. Griffiths, An Equivalent Model Using Discrete Element Method (DEM), Proc. 12th ASCE Engineering Mechanics Conf., La Jolla, CA, 1998.

(30) Buchanan, M.S., Evaluation of the Effect of Flat and Elongated Particles on the Performance of Hot Mix Asphalt Mixtures, NCAT Report No. 2000-03, May 2000.

(31) Maerz, N.H. and M. Lusher, Measurement of Flat and Elongation of Coarse Aggregate Using Digital Image Processing, Proc. 80th Transportation Research Board Meeting, Washington, D.C., 2001.

(32) Masad, E., Olcott, D., White, T. and L. Tashman, Correlation of Imaging Shape Indices of Fine Aggregate with Asphalt Mixture Perfomance, Proc. 80th Transportation Research Board Meeting, Washington, D.C., 2001.

(33) Ketcham, R.A. and N. Shashidhar, Quantitative Analysis of 3-D Images of Asphalt Concrete, Proc. 80th Transportation Research Board Meeting, Washington, D.C., 2001.

(34) Reddy, J.N., ***An Introduction to The Finite Element Method***, Second Edition, McGraw-Hill, 1993.